Cyclin C is a haploinsufficient tumor suppressor

Na Li[1], **Anne Fassl**[1], **Joel Chick**[2], **Hiroyuki Inuzuka**[3], **Xiaoyu Li**[4], **Marc R. Mansour**[5,6], **Lijun Liu**[1], **Haizhen Wang**[1], **Bryan King**[7], **Shavali Shaik**[3], **Alejandro Gutierrez**[5], **Alban Ordureau**[2], **Tobias Otto**[1], **Taras Kreslavsky**[4], **Lukas Baitsch**[8], **Leah Bury**[1], **Clifford A. Meyer**[9], **Nan Ke**[1], **Kristin A. Mulry**[1], **Michael J. Kluk**[10], **Moni Roy**[10], **Sunkyu Kim**[11], **Xiaowu Zhang**[12], **Yan Geng**[1], **Agnieszka Zagozdzon**[1], **Sarah Jenkinson**[6], **Rosemary E. Gale**[6], **David C. Linch**[6], **Jean J. Zhao**[8], **Charles G. Mullighan**[13], **J. Wade Harper**[2], **Jon C. Aster**[10], **Iannis Aifantis**[7], **Harald von Boehmer**[4], **Steven P. Gygi**[2], **Wenyi Wei**[3], **A. Thomas Look**[5], and **Piotr Sicinski**[1,15]

[1]Department of Cancer Biology, Dana-Farber Cancer Institute, and Department of Genetics, Harvard Medical School, Boston, Massachusetts 02215, USA.

[2]Department of Cell Biology, Harvard Medical School, Boston, Massachusetts 02115, USA.

[3]Department of Pathology, Beth Israel Deaconess Medical Center, Harvard Medical School, Boston, Massachusetts 02215, USA.

[4]Department of Cancer Immunology and AIDS, Dana-Farber Cancer Institute, and Department of Microbiology and Immunobiology, Harvard Medical School, Boston, Massachusetts 02215, USA.

[5]Department of Pediatric Oncology, Dana-Farber Cancer Institute, and Division of Hematology/ Oncology, Children's Hospital, Department of Pediatrics, Harvard Medical School, Boston, Massachusetts 02215, USA.

[6]Department of Haematology, University College London Cancer Institute, London WC1E 6BT, UK.

[7]Howard Hughes Medical Institute and Department of Pathology, NYU School of Medicine, New York, NY 10016, USA.

[8]Department of Cancer Biology, Dana-Farber Cancer Institute, and Department of Biological Chemistry and Molecular Pharmacology, Harvard Medical School, Boston, Massachusetts 02215, USA.

[9]Department of Biostatistics and Computational Biology, Dana-Farber Cancer Institute and Harvard School of Public Health, Boston, MA 02115, USA.

[10]Department of Pathology, Brigham and Women's Hospital, Boston, Massachusetts 02115, USA.

[11]Novartis Institutes for BioMedical Research, Cambridge, Massachusetts 02139, USA.

[12]Cell Signaling Technology, Inc., Danvers MA 01923, USA.

[13]Department of Pathology, St. Jude Research Hospital, Memphis, Tennessee 38105, USA.

Abstract

Cyclin C was cloned as a growth-promoting G1 cyclin, and was also shown to regulate gene transcription. Here we report that *in vivo* cyclin C acts as a haploinsufficient tumor suppressor, by controlling Notch1 oncogene levels. Cyclin C activates an "orphan" CDK19 kinase, as well as CDK8 and CDK3. These cyclin C-CDK complexes phosphorylate Notch1 intracellular domain (ICN1) and promote ICN1 degradation. Genetic ablation of cyclin C blocks ICN1 phosphorylation *in vivo*, thereby elevating ICN1 levels in cyclin C-knockout mice. Cyclin C ablation or heterozygosity collaborate with other oncogenic lesions and accelerate development of T-cell-acute lymphoblastic leukemia (T-ALL). Furthermore, the *cyclin C* gene is heterozygously deleted in a significant fraction of human T-ALL, and these tumors express reduced cyclin C levels. We also describe point mutations in human T-ALL that render cyclin C-CDK unable to phosphorylate ICN1. Hence, tumor cells may develop different strategies to evade cyclin C inhibitory function.

Cyclin C was cloned over 20 years ago as a growth promoting G1 cyclin, together with cyclins D and E[1, 2]. Whereas the D-type and E-type cyclins have been extensively studied, and their involvement in cancer is very well documented[3], the *in vivo* function of cyclin C remains largely unknown.

Several studies described a role for cyclin C in driving cell proliferation[4-8]. Cyclin C was shown to cooperate with c-Myc and postulated to function both in the G1 and G2 phases of the cell cycle[4]. Additional studies revealed a role for cyclin C during cell cycle re-entry from quiescence[6-8]. This function of cyclin C was attributed to the ability of cyclin C and its kinase partner, the cyclin-dependent kinase 3 (CDK3) to phosphorylate the retinoblastoma protein, pRB[7].

Most of studies, however, pointed to an essential role for cyclin C in transcription. Cyclin C together with its another catalytic partner CDK8 were identified as components of RNA polymerase II transcription initiation complexes. Cyclin C-CDK8 kinase was shown to repress transcription by phosphorylating the C-terminal domain (CTD) of the largest RNA polymerase II subunit[9-14], as well as by phosphorylating and inhibiting the general transcription factor TFIIH[15]. Moreover, cyclin C-CDK8 is incorporated into the inhibitory module of the transcriptional mediator complex, and sterically blocks the interaction of the

mediator complex with RNA polymerase II[16,17]. In addition to its function as a component of basal transcriptional machinery, cyclin C-CDK8 kinase was postulated to phosphorylate and negatively regulate the stability of sequence-specific transcription factors[18-21]. In contrast, other studies pointed to a positive role for cyclin C-CDK8 in mediating transcriptional activation, either as a part of basal transcriptional machinery, or downstream of p53, and of the Wnt/β-catenin pathway[22-26].

The human *CCNC* gene encoding cyclin C is located on chromosome 6q21, within the segment that is frequently deleted in several tumor types[27]. Indeed, heterozygous deletion of the *CCNC* gene was confirmed in human acute lymphoblastic leukemia[27] and osteosarcomas[28], and was postulated to play a role in tumorigenesis. However, other authors observed that the *CCNC* gene is amplified and overexpressed in human tumors[29-33].

To study the molecular role of cyclin C in a living organism, we generated conditional cyclin C knockout mice. We then used these mice to unravel the molecular functions of cyclin C *in vivo* in normal development and in tumorigenesis.

RESULTS

Phenotype of cyclin C-null embryos

Conditional cyclin knockout (cyclin $C^{F/F}$) mice were generated using standard procedures (Fig. 1a-c). We first converted the "floxed" cyclin C allele into cyclin C-null one (C) and evaluated the consequence of germline cyclin C ablation for embryonic development. Cyclin C-null (C $^{/}$) mice died *in utero* at embryonic day 10.5 (Fig. 1d). Gross and histopathological analyses revealed a severe developmental retardation of mutant embryos, and underdeveloped placental labyrinth layer (Fig. 1d,e).

Molecular analyses of cyclin C-null cells

In order to analyze the function of cyclin C at the molecular level, we derived embryonic fibroblasts (MEFs) from conditional cyclin C knockout mice and transduced them with Cre, thereby acutely deleting the cyclin C gene. We immunoprecipitated CDK8 and performed *in vitro* kinase assays using RNA polymerase II CTD as a substrate. The kinase activity of CDK8 was lost in cyclin C $^{/}$ cells (Fig. 2a), consistent with the notion that CDK8 is activated by cyclin C. However, phosphorylation of the endogenous CTD remained unaffected by cyclin C shutdown (Fig. 2b), revealing that other kinases are capable to maintain normal CTD phosphorylation levels.

Cyclin C together with CDK8 and MED12 and MED13 proteins forms an inhibitory mediator module, which sterically blocks interaction of the core mediator complex with RNA polymeraseII [16,17]. As expected, no interaction of cyclin C with MED12 and MED13 was observed in cyclin C-null cells (Fig. 2c, upper panel). Importantly, interaction of CDK8 with these proteins was also abolished upon shutdown of cyclin C (Fig. 2c, middle and lower panels), revealing that cyclin C is required for CDK8 incorporation to the inhibitory mediator module.

We next evaluated the effect of cyclin C ablation on gene expression, by comparing gene expression profiles between control and cyclin C $^{-/-}$ MEFs, embryonic stem cells and brains (the latter derived from E18.5 Nestin-Cre[34]/cyclin C$^{F/F}$ embryos), using microarrays. Shutdown of cyclin C had no major impact on global transcript levels (Fig. 2d,e), suggesting that cyclin C is not essential in controlling global transcription under normal conditions in the analyzed compartments.

To gauge the effect of cyclin C loss on cell proliferation, we compared growth rates between cyclin C$^{F/F}$ vs. C $^{-/-}$ MEFs. An acute ablation of cyclin C had no impact on cell growth (Fig. 3a). Moreover, cyclin C-null cells displayed unperturbed fractions of cells in G1, S and G2/M phases (Fig. 3b). However, cyclin C-null cells presented a defect in cell cycle re-entry from quiescence, especially when stimulated with lower concentrations of serum (Fig. 3c, left and middle panels). Importantly, genetic ablation of pRB fully restored the ability of cyclin C-null cells to re-enter the cell cycle (Fig. 3c right panel, compare cyclin C $^{-/-}$ vs. double-knockout C $^{-/-}$/Rb $^{-/-}$ cells). These observations suggest that pRB represents the rate-limiting target of cyclin C in cell cycle re-entry.

The function of cyclin C in cell cycle re-entry was proposed to be mediated by association with CDK3[7]. However, laboratory mouse strains contain a nonsense mutation within the *Cdk3* gene[35]. We observed that in mouse cells cyclin C interacts with related kinases Cdk1 and Cdk2 (Fig. 3d-f). Taken together, cyclin C is dispensable for continuous cell proliferation, but it plays a pRB-dependent role in cell cycle re-entry.

Upregulation of intracellular Notch1 (ICN1) following cyclin C ablation

To evaluate the impact of an acute cyclin C shutdown in a living mouse, we crossed cyclin C$^{F/F}$ mice with the Mx1-Cre strain and obtained cyclin C$^{F/F}$/Mx1-Cre animals. The Mx1-Cre strain expresses inducible Cre-recombinase; administration of polyinosinic-polycytidylic acid (pI-pC) to Mx1-Cre animals activates Cre in hematopoietic cells, leading to deletion of the "floxed" sequences[36] (Supplementary Fig. 1a). Unexpectedly, an acute ablation of cyclin C *in vivo* triggered enlargement of animals' thymi (Fig. 4a), and increased the number of thymocytes (Fig. 4b, and Supplementary Fig. 1b-d).

Immunoblot analysis of C $^{-/-}$ thymocytes revealed strongly increased levels of intracellular Notch1 (ICN1, Fig. 4c and Supplementary Fig. 1e,f). Importantly, the levels of Notch1 transcripts were unperturbed in cyclin C-null thymocytes (Fig. 4d), ruling out a transcriptional effect of cyclin C ablation on Notch1 levels. Moreover, the levels of full-length Notch1 protein as well as membrane-bound Notch1 were unchanged in cyclin C $^{-/-}$ thymocytes (Fig. 4c and data not shown), indicating that cyclin C specifically controls the protein levels of ICN1.

Ablation of cyclin C also led to strong upregulation of ICN1 in bone marrow cells (Fig. 4e), which displayed enhanced propensity to differentiate along the T-cell lineage (Supplementary Fig. 1g-j). Furthermore, when bone marrows of wild-type mice were reconstituted with 1:1 mixture of wild-type (CD45.1$^+$) and cyclin C $^{-/-}$ (CD45.2$^+$) hematopoietic progenitor cells, cyclin C-null cells strongly outcompeted wild-type cells in their contribution to the T-cell lineage, as expected from Notch1 activation (Fig. 4f).

A strong increase of ICN1 levels was not restricted to hematopoietic cells, as it was also observed in cyclin C $^{-/-}$ embryonic stem cells (Fig. 4g) and MEFs (Fig. 4h). Importantly, re-expression of cyclin C in cyclin C $^{-/-}$ MEFs restored normal ICN1 levels (Fig. 4i).

Cyclin C controls ICN1 stability *in vivo*

To understand the molecular basis of the increased ICN1 levels in cyclin C $^{-/-}$ cells, we cultured control and C $^{-/-}$ thymocytes in the presence of cycloheximide (to block protein synthesis) or with a γ-secretase inhibitor (to inhibit production of ICN1), and monitored the decay of ICN1 levels over time. Cyclin C ablation resulted in a significantly prolonged half-life of ICN1 (Supplementary Fig. 2a,b). Moreover, treatment of thymocytes with proteosomal inhibitors partially reversed the differences in ICN1 levels between control and C $^{-/-}$ cells (Supplementary Fig. 2c), indicating that defective ICN1 degradation may underlie the increased ICN1 levels in cyclin C-null cells.

To extend these studies to human cells, we depleted cyclin C in T-cell acute lymphoblastic leukemia (T-ALL) MOLT-16 cells using shRNAs. This led to strong upregulation of ICN1, without affecting the levels of full-length Notch1 (Fig. 4j and Supplementary Fig. 3a-d). Knockdown of cyclin C strongly stabilized ICN1 and prolonged its half-life (Supplementary Fig. 3c). Conversely, overexpression of cyclin C resulted in suppression of ICN1 levels, again without having any effect on full-length Notch1 (Supplementary Fig. 3e,f). Collectively, these analyses revealed that cyclin C acts as a rate-limiting repressor of intracellular Notch1 levels by affecting ICN1 protein-degradation rate.

Cyclin C-CDK8, C-CDK19 and C-CDK3 kinases phosphorylate ICN1

Shutdown of cyclin C in thymocytes led to disappearance of slower migrating ICN1 species (Supplementary Fig. 2c, compare lanes 3 vs. 4, and 5 vs. 6), suggesting that cyclin C might regulate ICN1 posttranslational modification. The enzymatic functions of cyclin C have been attributed to its kinase partners, CDK8 and CDK3[7,14]. Mammalian cells also express a CDK8-related "orphan" kinase, CDK19[37] (Supplementary Fig. 4a), for which the activating partner is unknown. We found that in MOLT-16 cells cyclin C physically interacts with CDK19 (Fig. 5a) and activates its kinase activity (Fig. 5e and Supplementary Fig. 4f,g). As expected, cyclin C also bound CDK8 and CDK3 in human cells (Fig. 5a). Knockdown of CDK8, CDK19 or CDK3 in human cells, and knockdown of CDK8 or CDK19 in mouse cells recapitulated the phenotype of cyclin C ablation, namely it upregulated ICN1 levels, without having any effect on full-length Notch1 (Fig. 5b,c and Supplementary Fig. 4b-e). Conversely, overexpression of CDK8, CDK19 or CDK3 strongly suppressed ICN1 levels without affecting full-length Notch1 (Supplementary Fig. 3e,f). These observations suggested that cyclin C controls ICN1 levels through its kinase partners CDK8, CDK19 and CDK3. Using purified, recombinant proteins, and proteins immunoprecipitated from cells, we found that cyclin C-CDK8, C-CDK19 and C-CDK3 complexes can phosphorylate ICN1 (Fig. 5d-f and Supplementary Fig. 4f-i).

Mapping of cyclin C-dependent phosphosites on ICN1, using mass spectrometry revealed that several of them are located within the PEST-domain of Notch1, which controls ICN1 degradation[38,39] (Fig. 5g and Supplementary Table 1). Three of them (T2512, S2514 and

S2517) are localized within the consensus motif, "Cdc4 phosphodegron", which is shared by most substrates of Fbw7 (Cdc4) ubiquitin ligase[38]. Two of these residues (S2514 and S2517) were previously shown by Fryer et al.[20] to be phosphorylated by cyclin C-CDK8 *in vitro*, and all three were shown to play a role in controlling ICN1 stability via Fbw7[40]. We verified that cyclin C-CDK8, C-CDK19 and C-CDK3 phosphorylate ICN1 on these three residues (Supplementary Fig. 5, Supplementary Tables 1,2).

We raised a phospho-specific antibody, which recognizes S2517-phosphorylated version of ICN1 (Supplementary Fig. 6a,b). Using this antibody we found that acute ablation of cyclin C inhibited phosphorylation of the endogenous ICN1 on this residue in cyclin C $^{/}$ thymocytes (Fig. 5h). Also knockdown of cyclin C in human T-ALL cells decreased S2517-phosphorylation of the endogenous ICN1 (Supplementary Fig. 6c). Hence, cyclin C-associated kinases control ICN1 phosphorylation *in vivo*.

Cyclin C-associated kinases regulate ICN1 polyubiquitination *in vivo*

Using recombinant proteins, we established that binding of ICN1 to Fbw7 is critically dependent on pre-phosphorylation of ICN1 by cyclin C-CDK kinase (Fig. 5i). Consistent with this, knockdown of cyclin C in human T-ALL cells, or ablation of cyclin C in MEFs decreased interaction of ICN1 and Fbw7 proteins *in vivo* (Supplementary Fig. 6c-f).

Interaction of ICN1 with Fbw7 leads to ICN1 polyubiquitination. Indeed, acute ablation of cyclin C strongly decreased polyubiquitination of the endogenous ICN1 in cyclin C-null thymocytes (Fig. 5j). Likewise, ubiquitination of ICN1 was reduced in human cells upon knockdown of cyclin C (Supplementary Fig. 6g).

Collectively, these findings support a model that cyclin C-CDK8/19/3 kinases phosphorylate ICN1 *in vivo* and allow binding of ICN1 to Fbw7, which then triggers ICN1 polyubiquitination and proteolytic degradation. Ablation of cyclin C disrupts this process, leading to upregulated ICN1 levels in cyclin C-null mice.

Increased susceptibility of cyclin C-deficient animals to T-ALL

Despite elevated ICN1 levels in bone marrow (Fig. 4e), cyclin C $^{/}$/Mx1-Cre mice did not spontaneously develop tumors. Prior work showed that elevations of ICN1 are not leukemogenic on their own, but promote development of T-ALL when combined with other oncogenic lesions[41]. We therefore tested whether cyclin C loss would enhance T-ALL development, by crossing C $^{/}$/Mx1-Cre animals with Lck-LMO1 transgenic mice. The LMO1 gene represents a recurring target of chromosomal translocations in human T-ALL[42]. Lck-LMO1 mice occasionally develop T-ALL after a long latency[43,44]. Importantly, activation of Notch1 represents an obligatory step in oncogenesis in this model[45,46]. We ablated cyclin C in cyclin C$^{F/F}$/LMO1/Mx1-Cre animals, and monitored them for tumor occurrence. Ablation of cyclin C strongly increased tumor incidence (Fig. 6a), and elevated ICN1 levels in cyclin C $^{/}$ tumors (Fig. 6b). These findings suggest that cyclin C may act as a tumor-suppressor in T-ALL by controlling ICN1 protein levels.

Transduction of murine hematopoietic progenitor cells (HPC) with viruses encoding very high levels of activated Notch1 is sufficient to trigger T-ALL without additional lesions[41]

(Supplementary Fig. 6c). We collected HPC from control and cyclin C $^{/}$ animals, and transduced them with oncogenic Notch1 alleles. The levels of ectopically expressed oncogenic Notch1 were strongly elevated in C $^{/}$ HPC, as compared to Notch1-transduced control HPC (Fig. 6d-f and Supplementary Fig. 7a,b). We then injected HPC into the bloodstream of sublethally irradiated C57BL/6 wild-type recipients and observed them for T-ALL occurrence (Supplementary Fig. 6c). The onset of leukemia was significantly accelerated in recipients of cyclin C $^{/}$ HPC (Fig. 6h and Supplementary Fig. 7c-e). Collectively, these observations indicate that the loss of cyclin C is not sufficient to trigger leukemia on its own, but it accelerates T-ALL development when combined with other genetic lesions.

We wished to confirm that the growth-suppressive role of cyclin C in T-ALL development is mediated through the ability of cyclin C–associated kinases to phosphorylate ICN1. We transduced control and C $^{/}$ HPC with an ICN1 mutant in which the domain containing the three critical cyclin C-dependent residues (T2512, S2514, S2517) had been deleted, and injected HPCs into recipient C57BL/6 mice. Strikingly, once the domain containing cyclin C-dependent phosphoresidues had been removed, ablation of cyclin C no longer accelerated T-ALL development (Supplementary Fig. 7f). Hence, the tumor-suppressive role of cyclin C *in vivo* is mediated through the ability of cyclin C to phosphorylate Notch1.

Cyclin C heterozygosity accelerates T-ALL

The cyclin C gene (*CCNC*) is located on 6q21 within a region that is frequently deleted in breast, ovarian, prostate, and lung cancers, osteosarcomas and in hematopoietic malignancies, including T-ALL[47-50]. Heterozygous deletion of *CCNC* was verified in leukemias and osteosarcomas, and proposed to contribute to tumorigenesis[27,28]. Given the rate-limiting role of cyclin C in controlling ICN1 levels *in vivo*, demonstrated in this study, we analyzed primary T-ALL patient samples and human T-ALL cell lines using array-comparative genomic hybridization (CGH). Chromosomal deletions involving *CCNC* were found in 13/150 primary patient samples and in 4/20 T-ALL cell lines (Fig. 7a,b). Sequencing of the remaining cyclin C allele revealed no mutations in the coding sequence. However, the levels of cyclin C transcripts were reduced approximately two-fold in T-ALL cases that sustained *CCNC* heterozygous deletion (Fig. 7c). These observations hinted that cyclin C haploinsufficiency might contribute to T-ALL development. Intriguingly, the CDK19 gene is also located on 6q21 in close proximity to *CCNC* (within 10Mb), and it is hence often co-deleted with *CCNC* (see also Supplementary Fig. 7g).

To test whether heterozygosity at the cyclin C locus might contribute to tumorigenesis *in vivo*, we collected HPC from heterozygous cyclin C$^{+/}$ /Mx1-Cre animals. These cells expressed reduced levels of cyclin C, and elevated levels of endogenous ICN1 (Fig. 6d and Supplementary Fig. 7a,b). We then transduced cyclin C$^{+/}$ HPC with oncogenic Notch1. As was the case in cyclin C-null HPC, the levels of oncogenic ICN1 were elevated in C$^{+/}$ HPC, as compared to Notch1-transduced control cells (Fig. 6g). We injected HPC into recipient mice and observed them for tumor development. Strikingly, cyclin C heterozygosity accelerated T-ALL development to almost the same extent as a complete cyclin C loss (Fig. 6i). These results indicate that cyclin C represents a haploinsufficient

tumor-suppressor, and that the loss of one cyclin C allele is sufficient to accelerate leukemia *in vivo*.

ICN1 mutations accelerate T-ALL by blocking cyclin C-dependent phosphorylation

We wished to determine whether in addition to *CCNC* deletions, the ability of cyclin C-CDK to phosphorylate ICN1 could be compromised in human T-ALL through other mechanisms. Since CDKs are proline-directed kinases[37], we analyzed our DNA sequencing data of the *NOTCH1* gene from 73 T-ALL patients[51] and searched for mutations in prolines adjacent to critical cyclin C-CDK-dependent phosphoresidues of ICN1 identified above. We observed four cases with substitutions involving proline residues: P2513A, P2513S, P2513L and P2515R, and one additional case with S2514 mutated to phenylalanine (Fig. 8a). We determined that each of these mutations severely crippled the ability of cyclin C-CDK8 to phosphorylate ICN1 on all three or on two out of three critical residues (Fig. 8b,c, and Supplementary Table 3). As expected from decreased phosphorylation, all five patient-derived Notch1 mutants showed greatly reduced interaction with Fbw7 (Fig. 8d-e).

To evaluate the impact of these patient-derived mutations on tumorigenesis *in vivo*, we engineered a weakly oncogenic Notch1-P12 allele[41] to express S2514F mutation, or a combination of three patient-derived mutations (P2515R, P2513A, S2514F). We then transduced wild-type HPC with viruses encoding these Notch1 alleles, and injected HPC into C57BL/6 recipients. The disease was accelerated in recipients of S2514F Notch1-transduced cells, whereas the compound mutant dramatically accelerated the disease (Fig. 8f). Collectively, these results indicate that mutations that cripple the ability of cyclin C-CDK kinase to phosphorylate ICN1 contribute to T-ALL development *in vivo*.

DISCUSSION

Cyclin C was cloned as a protein that promotes cell cycle progression through the G1 phase[1,2]. Subsequent studies revealed that cyclin C represents a component of global transcriptional machinery, and that it represses gene expression[9-15]. Surprisingly, we found that the major, rate-limiting function of cyclin C *in vivo* in the hematopoietic lineage is to suppress ICN1 levels. We demonstrated that cyclin C-CDK19, C-CDK8 and C-CDK3 complexes serve as *in vivo* repressors of Notch1 by directly phosphorylating ICN1. Ablation of cyclin C, or cyclin C heterozygosity lead to de-repression of ICN1 levels and accelerate T-ALL development. Thus, cyclin C acts to restrain proliferation of the T-cell lineage and functions as a growth-suppressor. Furthermore, we describe point mutations in human tumors that render cyclin C-CDK unable to phosphorylate ICN1. These observations indicate that human T-ALL cells employ different strategies to disable cyclin C function.

Activation of Notch1 represents a driving force not only in T-ALL, but also in many other cancer types[52]. Deletions of 6q21 where the *CCNC* gene resides are seen in several human malignancies, including breast, prostate and lung cancers, as well as several types of leukemias and lymphomas[27,28,47-50,53,54]. It remains to be seen whether cyclin C plays a tumor-suppressive role in other cancer types, and whether this function is mediated via Notch1. Crossing of cyclin C[F/F] mice with strains expressing Cre in different compartments, along with analyses of human tumors will help to address this point.

It should be noted, however, that Notch1 can also function as a tumor-suppressor, depending on the cellular context[55]. For example, Notch1 represents a well-established tumor-suppressor in human squamous cell carcinoma[56-58]. It remains to be seen whether cyclin C can regulate ICN1 levels also in this context and, if so, whether it functions as an oncogene in some tumor types.

In addition to controlling Notch1 levels, cyclin C plays a pRB-dependent role in facilitating G_0 exit[6-8]. Indeed, we observed modestly impaired ability of cyclin C-null cells to re-enter the cell cycle. This function of cyclin C might promote tumorigenesis in certain compartments, in particular under circumstances where quiescent tumor-initiating cells enter the G1 phase. Cyclin C may also affect cancer cells through other mechanisms. Indeed, in distinction to an anti-proliferative role of cyclin C-CDK8 in the T-cell lineage, demonstrated in this study, CDK8 was shown to function as an oncogene in human colon cancers, where it promotes β-catenin-driven transcriptional activity and stimulates cell proliferation[23,24]. Hence, CDK8 kinase represents an attractive target for therapeutic intervention in colon cancers. However, our study cautions that using CDK8-inhibitors for colon cancer treatment may elicit pro-tumorigenic effects in other compartments.

METHODS

Generation of conditional cyclin C knockout mice

Conditional cyclin C gene targeting construct was assembled by inserting *loxP* sites into the PvuII site in intron 1 and into the KpnI site in intron 7 of murine *cyclin C* gene. In addition, a Neomycin resistance (Neo) cassette, flanked by two *FRT* sites, was inserted into the PvuII site in intron 1. The 5' homology arm comprised a 2.2kb SalI-PvuII fragment, and the 3' arm a 4 kb KpnI – BmgBI fragment of the *cyclin C* gene. The targeting construct was electroporated into ES cells, and cells that underwent homologous recombination were identified using Southern blotting with external probes (probes A and B in Fig. 1) and EcoRI digest of genomic ES cell DNA. Heterozygous animals were obtained using standard procedures. Animals were then bred with ACTFLPe mice (from the Jackson Laboratory) leading to deletion of the Neo cassette and to generation of cyclin $C^{+/F}$ mice. Cyclin $C^{+/F}$ mice were then interbred, giving rise to conditional knockout cyclin $C^{F/F}$ mice. For genotyping animals, the following PCR primers were used: P1: 5'-GGGGTGATGGTGAAAACACTGA-3', P2: 5'-CAAGCAAGTAATCCAGGACCA-3' and P3: 5'-CTGCACATACTGGAGCAAAGGTCT-3' (see Fig. 1a, c). PCR was performed with a denaturation step at 95°C for 3 min, followed by 30 cycles of 95°C – 1 min, 60°C – 1 min, 72°C – 1 min, and a final elongation step at 72°C for 5 min. The wild-type cyclin C^+ allele yields a 460 bp band, the cyclin C^F allele a 520 bp band, and the cyclin C allele a 650 bp band.

Mouse crosses and analyses

All mouse experiments were approved by the Dana-Farber Cancer Institute Animal Care and Users Committee. Cyclin $C^{F/F}$ mice were crossed with Mx1-Cre mice[36] (from the Jackson Laboratory). Four to six weeks old $C^{F/F}$/Mx1-Cre⁻ (control), $C^{+/F}$/Mx1-Cre and $C^{F/F}$/Mx1-Cre mice were intraperitoneally injected five times with polyinosinic–polycytidylic acid (pI-

pC, Amersham), 2.5 µg/g body weight on alternate days. Organs (thymuses, bone marrow) were collected 5 to 10 days after the last pI-pC dose and analyzed by flow cytometry, or used to prepare protein lysates, for *in vitro* treatment of thymocytes. Thymocytes were stained with anti-CD4, anti-CD8, anti-CD25 (all from BD Pharmingen) and anti-CD44 (Biolegend) antibodies, and analyzed by FACS.

Cyclin $C^{F/F}$/Mx1-Cre$^-$ and Mx1-Cre mice were also crossed with LMO1 transgenic strain[44] yielding $C^{F/F}$/LMO1+/Mx1-Cre$^-$ (control) and $C^{F/F}$/LMO1+/Mx-Cre mice. Animals were injected with pI-pC, as above, at about 4-6 weeks of age, and were monitored for leukemia occurrence by analysis of peripheral blood.

For isolation of MEFs, cyclin $C^{F/F}$ mice were crossed with $pRb^{F/F}$ mice (from the Jackson Laboratory). To delete cyclin C in the brain, cyclin $C^{F/F}$ mice were crossed with Nestin-Cre animals[34]. Brains were then collected from E18.5 cyclin $C^{F/F}$/Nestin-Cre mice.

The sample size was chosen based on our extensive experience in analyzing phenotypes and tumor susceptibility of mice from a homogenous, inbred background (no statistical method). All differences were tested for statistical significance (please see "Statistical analyses" below). No animals were excluded from the analysis. No randomization was used to determine how animals were allocated to experimental groups. The investigators were not blinded to group allocation. Mice were of the 129Sv/C57BL/6 background. For all experiments mice of both sexes, 6-12 weeks old were used, unless indicated otherwise in figure legend.

Generation of mixed bone marrow chimeras

Bone marrow cells from CD45.1 wild-type and CD45.2 cyclin $C^{/}$/Mx1-Cre mice (approx. 2 weeks after the last pI-pC dose) or from CD45.2 wild-type mice, were stained with CD4, CD8α, TCRβ, TCRγδ, and NK1.1 biotinylated antibodies followed by incubation with streptavidin-conjugated magnetic beads (Invitrogen) and magnetic bead depletion of T and NK cells. CD45.1 C57BL/6 recipients were subjected to lethal irradiation (1000 rads) using a γ-cell 40 irradiator with a cesium source. Mixed (1:1) T cell- and NK-cell-depleted bone marrow cells (4–8×10^6) were intra-orbitally injected into the recipient mice. Chimeras were analyzed at 11 weeks after the bone marrow transfer.

Retrovirus production and bone marrow transplantation

Murine Notch1-expressing ICN1-EGFP and pMigR1-Notch1-P12 retroviral constructs were described previously[59,60]. Notch1-P12 mutants S2514F and P2513A/S2514F/P2515R were generated with the QuikChange II XL Site-Directed Mutageneis kit (Stratagene). Retroviruses were produced by transient co-transfection of 293T or PlatE cells with Notch1-expressing constructs and appropriate packaging vectors as described previously. The titration of retroviruses was performed in NIH3T3 cells. Donor $C^{F/F}$/Mx1-Cre$^-$, $C^{+/F}$/Mx1-Cre, and $C^{F/F}$/Mx1-Cre mice were injected 3 to 5 times with pI-pC. Bone marrow was collected 5-10 days after the last pI-pC dose. Retroviral transduction and bone marrow transplantation were carried out as follows: Lineage negative (CD3ε, TCR-ß, NK1.1, DX5, CD19, Ter-119, Mac-1 and Gr-1) bone marrow cells were sorted and cultured with Flt3L,

SCF (both 50 ng/ml), IL-6, IL-7, and IL-3 (10 ng/ml) (all from R&D Systems). On day 2 and day 4 after cell sorting, cells were subjected to retroviral transduction by spin infection with centrifugation at 2300rpm for 1.5 hrs at room temperature with 8 μg/ml polybrene. On day 5, $1\text{-}2\times10^6$ cells were injected intravenously into sub-lethally irradiated C57BL/6 recipient mice. Alternatively, cells were spin infected at 700g for 1.5 hrs at 30°C on days 1 and 2, and 50,000 GFP$^+$ cells were retroorbitally injected into irradiated recipients on day 3. In experiment shown in Supplementary Fig. 7f, ΔEGF ΔLNR Notch1 construct lacking amino acids 23-1562 and 2473 to 2556 (ref.61) was used for bone marrow transduction. Animals were monitored for leukemia occurrence by analysis of peripheral blood. Peripheral blood GFP$^+$ cells were stained with anti-CD4 and anti-CD8 antibodies as above, and analyzed by FACS.

For analyses of Notch1-P12 levels (Fig. 6e-g), pI-pC-treated mice received one dose of 5-FU (150 mg/kg) 4 days after the last pI-pC dose. Bone marrow cells were harvested 6 days later and transduced with a retrovirus expressing Notch1-P12 and GFP. GFP$^+$ cells were sorted, and used for immunoblotting.

In vitro culture and analyses of bone marrow cells

To analyze bone marrow or thymocyte subpopulations, single cell suspensions were prepared from bone marrow collected from femur and tibia or were isolated from the whole thymus. Cells were blocked with rat IgG (Sigma), stained with fluorescently conjugated antibodies in PBS/2% FCS on ice for 30 min, and analyzed using a BD Fortessa. FACS plots were generated and quantified using FlowJo software (Treestar). Bone marrow cells were stained for lineage markers: B220 (RA3-6B2), Gr1 (RB6-8C5), CD11b (M1/70), Ter119, CD4 (GK1.5) and CD8 (53-6.7), as well as c-kit (2B8), Sca1 (D7), CD34 (RAM34) and Flt3 (A2F10). Sub-populations were defined as follows: LT-HSC: Lin$^-$, c-kit$^+$, Sca1$^+$, CD34$^-$, Flt3$^-$; ST-HSC: Lin$^-$, c-kit$^+$, Sca1$^+$, CD34$^+$, Flt3$^-$; LMPP: Lin$^-$, c-kit$^+$, Sca1$^+$, CD34$^+$, Flt3$^+$; CLP: Lin$^-$, ckit^{lo}, Sca1^{lo}, Flt3$^+$, IL7Rα$^+$. To determine thymocyte subpopulations, thymocytes were stained for CD4 (GK1.5), CD8 (53-6.7), CD25 (PC61) and CD44 (IM7). Double-negative (CD4$^-$CD8$^-$) thymocyte populations were sub-classified as follows: DN1: CD25$^-$, CD44^{hi}; DN2: CD25$^+$, CD44$^+$; DN3: CD25$^+$, CD44$^-$; DN3-4: CD25^{int}, CD44$^-$; DN4: CD25$^-$, CD44$^-$. All antibodies were purchased from eBioscience, BD Biosciences or BioLegend.

To perform *in vitro* analyses, Lin$^-$ bone marrow cells were cultured in Opti-MEM supplemented with 10% FCS, Flt3L (5 ng/ml) and IL-7 (1 ng/ml) either alone or co-cultured on a layer of OP9 stromal cells overexpressing delta-like 1 (DLL1) protein (OP9-DL1). In Fig. 6d and Supplementary Fig. 7a, cells were cultured for 48 h on OP9-DL1 stroma. To quantify proliferation, bromodeoxyuridine (BrdU, 10 μM) was added to the cultures for 1 hr; cells were stained using BrdU Flow Kit (BD Biosciences) and analyzed by flow cytometry.

Immunostaining

Standard 4-micron formalin-fixed, paraffin embedded tissue sections were stained using the Ventana Benchmark XT platform (Ventana Medical Systems) with extended heat-induced epitope retrieval (CC1 Buffer). Slides were incubated for 1 hr at room temperature with anti-

NICD1 rabbit monoclonal antibody (clone D3B8, catalog #4147, Cell Signaling, final concentration, 8.5 μg/ml). Signals were then amplified (Ventana Amplification Kit) and visualized (Ventana Ultraview Universal DAB detection kit).

Western blotting and immunoprecipitation

Whole cell extracts were obtained and proteins were solubilized for immunoblotting. The following antibodies were used: cyclin C (A301-989A, Bethyl, 1:500 or 1:1000), CDK8 (C-19, Santa Cruz, 1:200-1:1000), CDK19 (HPA007053, Sigma, 1:1000 or 1:2000), CDK3 (SC-826, Santa Cruz, 1:200), CDK1 (Ab-1, Thermo Scientific, 1:200), CDK2 (M2, Santa Cruz, 1:500), Notch ICN1 (V1744, Abcam, 1:500 or 1:1000), Notch1 ICN1 (2421, Cell Signaling, 1:500 or 1:1000), Notch1 full-length and membrane-bound (C-20, Santa Cruz, 1:500 or 1:1000), c-Myc (9E10, Santa Cruz and ABC, Cell Signaling 1:500 or 1:1000), FBW7 (A301-720A, Bethyl, 1:2000), HA (A190-108A-4, Bethyl, 1:500), cyclin E1 (M-20, Santa Cruz, 1:500 or 1:2000), His-probe (H-20, Santa Cruz, 1:300), GST (2622S, Cell Signaling, 1:1000), GAPDH (D16H11, Cell Signaling 1:1000), tubulin (DM1A, Sigma, 1:2000 or 1:5000), actin (AC40, Sigma, 1:3000), β-actin (AC-15, Thermo Scientific, 1:5000; or 4967, Cell Signaling, 1:1000), CDK6 (C-21, Santa Cruz, 1:500), MCL1 (S19, Santa Cruz, 1:500 or 1:1000), mTOR (2972, Cell Signaling, 1:1000), c-Jun (9162, Cell signaling 1:500), pRB-pS807/811 (D20B12, Cell Signaling, 1:1000), MED12 (A300-774A-1, Bethyl, 1:500), MED13 (A301-278A-1, Bethyl, 1:500), phospho-Rpb1 CTD (Ser2/5) (4735S, Cell Signaling, 1:500), RNA polymerase II (05-623B, clone CTD4H8, Upstate 1:500), Flag (M2, Sigma, 1:1000 or 1:4000), ubiquitin (Z0458, Dako, 1:2000). Cross-linked anti-c-Myc antibody (9B11, Cell Signaling, 8 μl slurry) was used for immunoprecipitation (IP).

For IP of endogenous ICN1 from MOLT-16 cells, 2 mg of MOLT16 cell extracts were incubated with 2 μg Notch ICN1 antibody (ab52301, Abcam) for 12 hrs at 4°C followed by 1h incubation with protein A sepharose beads (GE Healthcare). For IP of endogenous ICN1 from thymocytes, thymocytes were collected from $C^{F/F}$/Mx1-Cre$^-$ and $C^{/}$/Mx1-Cre mice, and cultured in the presence of MG132 (10 μM) for 6 hrs. Protein extracts were prepared, and extracts containing 2 mg of proteins were immunoprecipitated with anti-cleaved Notch1 (Val1744) antibody (4147; Cell Signaling, 1:200) overnight at 4°C, followed by 3 hrs incubation with protein A agarose beads (Cell Signaling). Blotting with an anti-phospho-ICN1 (1:1000) and total ICN1 (2421, Cell Signaling 1:500) antibodies, shown in Fig. 5h are from separate immunoprecipitations. Immunocomplexes were resolved on SDS-PAGE gels. Immunoreactive proteins were detected using enhanced chemiluminescence reagents (GE Healthcare).

Generation of anti-phospho ICN1 antibody

Anti-phospho-Notch1 antibody was generated by Cell Signaling Technologies, Inc., by immunizing rabbits with peptides that were phosphorylated on both S2514 and S2517. Affinity-purified antibody was tested by immunoblotting protein lysates with anti-phospho-ICN1 antibody (1:1000), or by immunoprecipitating ICN1 – immunoblotting with anti-phospho-ICN1 antibody using lysates of cells engineered by us to express wild-type ICN1, ICN1-T2512A, ICN1-S2514A, ICN1-S2517A, ICN1-S2514A/2517A and ICN1- T2512A/ S2514A/2517A mutants. Mutation of S2517 to alanine completely abolished

immunoreactivity with anti-phospho-ICN1 antibody. On the other hand, mutating S2514 (or T2512) had no impact on the ability of anti-phospho-ICN1 antibody to detect ICN1 (Supplementary Fig. 6a,b). Moreover, treatment of ICN1 immunoprecipitates with lambda phosphatase abolished the immunoreactivity (Supplementary Fig. 6b, lower panel). We concluded that anti-phospho-ICN1 antibody recognizes ICN1 phosphorylated on Serine 2517. The antibody was used at 1:1000 dilution.

Plasmids

HA-FBW7, shFBW7 lentiviral vectors were described previously[62]. pcDNA3-CDK8-HA and pBabe-puro-CDK8 were purchased from Addgene. pmigRI-ΔELNotch1 retroviral vector and pcDNA3-ICN1 were described previously[61]. All Notch1 ICN1 mutants were generated with the QuikChange XL Site-Directed Mutagenesis kit (Stratagene). Lentiviral shRNA control constructs against GFP (CTR) and against human cyclin C (shCycC1: NM_005190.2-282s1c1, shCycC2: NM_005190.2-114s1c1, shCycC3:NM_005190.2-843s1c1) were obtained from Dr. William Hahn (Dana-Farber Cancer Institute), against human CDK8, CDK3 and CDK19 were purchased from Open Biosystems, control construct against GFP (CTR in Fig. 5b,c) was obtained from Dr. Fabienne Schmit (Dana-Farber Cancer Institute), against mouse CDK8 (Cdk8-sh1: NM_153599.2-1104s1c1, Cdk8-sh2: NM_153599.3-1893s21c1) and CDK19 (Cdk19-sh1: NM_198164.1-955s1c1, Cdk19-sh2: NM_198164.2-624s21c1, Cdk19-sh3: NM_198164.1-1491s1c1) were obtained from the TRC shRNA library. PmigICN1 retrovirus vector was generated by subcloning human ICN1 cDNA into PmigII vector. GST-ICN1 was generated by subcloning human ICN1 cDNA into PGEX5.1 vector. Lentiviral CDK expression plasmids were constructed by subcloning human CDK8, CDK3 or CDK19 cDNA into pLenti-GFP-puro vector. pFN18A-Halo-TUBE plasmid was obtained from Prof. Sir Philip Cohen (MRCPPU, Dundee, U.K)

Cell culture

Thymocytes were cultured in RPMI1640 with 10% FCS. Cells were treated with proteasome inhibitor MG132 (10 μM; Calbiochem) and lactacystin (10 μM; Enzo), or with vehicle only (DMSO) six hours before protein extraction. For ICN1 half-life studies, cycloheximide (20 μg/ml, Sigma) or γ-secretase inhibitor Compound E (200 nmol, Enzo) was added to the media, and cells were harvested at the indicated time-points.

Cyclin C$^{F/F}$ MEFs were prepared from E13.5 embryos. For experiments with ICN1-expression, cells were immortalized with dominant-negative p53 construct. Cells were treated with AdenoCre (MOI 100, Harvard Gene Therapy Initiative) to delete cyclin C and to generate cyclin C$^{-/-}$ cells. For control, cyclin C$^{F/F}$ MEFs were treated with adenovirus expressing empty vector. For Notch1 expression in MEFs, cyclin C$^{F/F}$ cells were infected with p-Mig-ICN1-Myc retrovirus (Supplementary Fig. 6d) or pmig-ΔELNotch1GFP expressing human Notch1 without the EGF-like repeats 1 to 36 and the three Lin12/Notch repeats (residues R23 to C1562) (Fig. 4h,i, 5b,c, and Supplementary Fig. 6f). Subsequently, cells were treated with adenoviruses expressing Cre (MOI 100), or empty vector. In Fig. 4i, cyclin C$^{F/F}$ MEFs were engineered to stably express cyclin C, using pOZ-FH-N expression vector, and then were transduced with pmig-ΔELNotch1GFP retrovirus. Cells were then

treated with adenoviruses expressing Cre (C$^{/}$), or empty vector (C$^{F/F}$). In experiment shown in Supplementary Fig. 6f, a mutant version of Notch1 (TSS: T2512A/S2514A/S2517A) was used. In Supplementary Fig. 6d, cells were treated with 10 μM MG132 for 6-10 hrs before protein extraction. In experiments shown in Fig. 5b,c, cyclin C$^{F/F}$ MEFs were infected with pMigRI-ΔEΔLNotch1GFP retroviral vector. Subsequently, cells were transduced with lentiviruses encoding shRNAs targeting murine CDK8 or CDK19 and selected with puromycin. Cells were harvested 72 hrs after lentiviral infection.

HeLa cells (ATCC) were maintained in DMEM (Invitrogen) supplemented with 10% FCS (Invitrogen). Cells were co-transfected with plasmids encoding ICN1-Myc (plasmid pcDNA3-ICN1-myc) or the indicated ICN1 point-mutants together with HA-tagged FBW7 (Fig. 8e and Supplementary Fig. 6e; cells were treated with proteasome inhibitor MG132 before harvesting).

MOLT16 cells were cultured in RPMI1640 with 10% FCS. Cells were transduced with lentiviruses encoding control shRNAs or shRNAs against cyclin C, FBW7, CDK8, CDK19, or CDK3, and selected with puromycin. Alternatively, cells were transduced with retroviruses encoding empty vector, or human cyclin C, CDK8, CDK19 or CDK3 cDNA (plasmids pCDNA3-CDK-HA) and selected with puromycin (Suplementary Fig. 3f).

MOLT-4 cells were transduced with MSCV-IRES-GFP, MSCV-ICN1-WT-IRES-GFP (encoding C-terminally Myc-tagged wild-type ICN1), or MSCV-ICN1-P2515R-IRES-GFP (encoding C-terminally Myc-tagged ICN1- P2515R). GFP^{low} cells were sorted by FACS. Prior to analyses, protein lysates were prepared with RIPA buffer, and immunoblotted with anti-Notch1 (D1E11, Cell Signaling, 1:1000), anti-GFP (Clones 7.1/13.1, Roche, 1:1000), and anti-Myc (71D10, Cell Signaling, 1:1000) antibodies, to ascertain that Myc-tagged ICN1 was expressed at approximately the same level as the endogenous ICN1.

Cell lines were from ATCC or DSMZ and were tested for mycoplasma.

Cell cycle analysis

Cells were labeled with 10 μM BrdU for 60 min, fixed in 80% ethanol, stained using FITC-labeled anti-BrdU antibody (556028, BD, 1:5) and 10 μg/ml propidium iodide, and analyzed on a LSR II flow cytometer (BD). For cell cycle re-entry analyses shown in Fig. 3c, MEFs were kept in DMEM without serum for 48 hrs, and then stimulated with DMEM plus the indicated concentrations of serum (FCS).

Real-time RT-PCR analysis

RNA was extracted using RNeasy Mini Kit (Qiagen), and the reverse transcription (RT) reaction was performed using First Strand cDNA Synthesis Kit (GE Health Care). After mixing the resultant template with Notch1- or HPRT-specific primers and with SYBR green PCR master mix (Applied Biosystems), PCR was performed with 7300 Real Time PCR System (Applied Biosystems). Oligonucleotide primer sequences were as follows: Notch1 primers: Notch1-F: 5'-TGAGACTGCCAAAGTGTTGC-3'; Notch1-R: 5'-GTGGGAGACAGAGTGGGTGT-3; HPRT primers: HPRT-F: 5'-CCTCTGGTAGATTGTCGCTT-3; HPRT-R: 5' GAGAGCTTCAGACTCGTCTA-3.

In vivo polyubiquitination detection

For analysis of polyubiquitination of the endogenous ICN1 (Fig. 5j), thymuses were harvested from cyclin $C^{F/F}$/Mx1-Cre and $C^{\prime}$/Mx1-Cre mice, and thymocytes were cultured with MG132 (10 μM) for 6 hrs. Protein extracts were prepared in lysis buffer containing 100 mM Iodoacetamide. Polyubiquitylated proteins were captured from cell extracts (containing 3.5 mg of protein) with Halo-TUBE as described previously[63]. Captured proteins were resolved on SDS-PAGE along with whole cell extract and immunoblotted with the indicated antibodies.

For analyses shown in Supplementary Fig. 6g, 293 cells were infected with lentiviral shRNA against GFP or cyclin C, and selected with puromycin. Knock-down cell lines were transfected with pCDNA3-ICN1-Myc and His-Ub. 36 hrs after transfection, cells were treated with 25 μM MG132 for 6 hrs prior to protein extraction. Extracts were incubated with Ni-NTA matrices at room temperature for 3 hrs in the presence of 6 M guanidine-HCl, pH8.0. Immobilized proteins were resolved by SDS-PAGE and immunoblotted with an anti-Myc antibody.

Expression and purification of recombinant GST-ICN1 protein from bacteria

GST-ICN1 was expressed in BL-21 (DE3) bacteria. Expression of recombinant proteins was induced with 0.1mM IPTG for 6 hrs at 37°C. Bacteria were lysed by sonication in PBS pH 7.4 containing 1% N-Lauroyl sarcosine, 1mM EDTA, 10mM DTT and protease inhibitors, and GST-ICN1 protein was purified on glutathione beads. GST-ICN1 was then eluted from the beads with 25mM glutathione, 200 mM NaCl, 50 mM Tris pH 8.8, dialyzed in kinase buffer and concentrated before the kinase reaction.

Expression and purification of recombinant cyclin C-CDK kinases from Sf9 cells

Human CDK19 and CDK3 cDNAs (both from Addgene) and human cyclin C cDNA were cloned into pTriEx-5™ vector (from Dr. Thomas Roberts, Dana- Farber Cancer Institute) using the following primers: 5'-GGGGGTACCCGATTATGATTTCAAGGCGAAGCT-3' and 5' GGGAAGCTTGTACCGGTGGGCCTGGTGA-3' (CDK19); 5'-GGGGGATCCGGATATGTTCCAGAAGGTAGAG-3' and 5'-GGGAAGCTTATGGCGGAATCGCTGCAGCA-3' (CDK3); 5'-GGGGGATCCGGCAGGGAACTTTTGGCAGAG-3' and 5'-GGGAAGCTTAGATTGGCTGTAGCTAGAGTTCT-3' (cyclin C).

Sf9 cells were maintained in BacVector Insect cell medium. CDK19, CDK3, and cyclin C in pTriEx™ vectors (0.5 μg each) were individually co-transfected with BacMagic DNA into Sf9 cells using BacMagic™ Transfection Kit (Novagen). Medium containing recombinant baculovirus (~1×10^7pfu/ml) was harvested after 5 days. Supernatants were then used to infect/co-infect Sf9 cells for 48 hrs to generate His-tagged cyclin C, cyclin C-CDK19, and cyclin C-CDK3. I-PER Insect Cell Protein Extraction Reagent (Thermo Scientific) supplemented with protease inhibitors was used to lyse insect cells, and kinase complexes were purified using an anti-His antibody immobilized on Protein A/G Plus-Agarose beads (Santa Cruz).

Expression and purification of recombinant cyclin C-CDK kinases from HEK293 cells

Mammalian expression vectors encoding His-tagged human CDK19 (pTriEx-5) and cyclin C (pCMV Sport6), or HA-tagged human CDK3 (pcDNA3) and cyclin C, or only His-tagged CDK19, only HA-tagged CDK3 or only cyclin C, were co-transfected into HEK293 cells using Lipofectamine 2000 (Invitrogen). Cells were harvested after 48 hrs, sonicated and lysed in kinase buffer without ATP added. Anti-His antibody immobilized on Protein A/G Plus-Agarose beads (Santa Cruz) was used to purify His-CDK19-cyclin C protein complexes or His-CDK19. Anti-HA antibody immobilized on Protein A/G Plus-Agarose beads was used to purify HA-CDK3-cyclin C protein complexes or HA-CDK3.

In vitro kinase reactions

For cyclin C-CDK8 kinase assays, 0.1 μg of cyclin C-CDK8 (Life Technologies, PV4402) and 1 μg of GST-ICN1 protein immobilized on glutathione-Sepharose beads were used. For cyclin C-CDK19 and C-CDK3 assays, cyclin C-CDK complexes were purified from Sf9 or HEK293 cells as described above and used together with 0.5 μg of GST-ICN1. Kinase assays were performed in a final volume of 30 μl of kinase buffer (50 mM HEPES pH 7.5, 10 mM $MgCl_2$, 1 mM DTT, 1 mM EGTA, 0.1 mM NaF) containing 10 μM ATP and 0.4 mCi [γ-^{32}P] ATP. After a 30 min incubation at 30°C, proteins were resolved on SDS-PAGE gels and analyzed by autoradiography.

For mass spectrometric analyses (Supplementary Fig. 5), cyclin C-CDK19 or C-CDK3 complexes, purified from Sf9 cells, were incubated with 0.1 μg of the peptide N-EHPFLTPSPESPDQWFPK-C (from NeoBioLab), corresponding to amino acids 2507 to 2521 of Notch1, in 30 μl of kinase reaction mixture for 30 min at 30°C. Samples were then analyzed by mass spectrometry.

In vitro and *in vivo* Fbw7 binding assays

Fbw7 *in vitro* binding to immobilized GST-fusion proteins was performed as described previously[62]. Where indicated, GST-ICN1 fusion proteins were incubated with recombinant cyclin C-CDK8 (Invitrogen) in the presence of 0.2 μM cold ATP for 1 hr prior to binding assays.

For *in vivo* binding assays, HeLa cells were transfected with an empty vector (EV) or Myc-tagged wild-type ICN1 or various ICN1 mutants along with HA-tagged Fbw7. 20 hrs after transfection, cells were treated with 15 μM MG132 overnight before harvesting for immunoprecipitation. Protein extracts were subjected to immunoprecipitation with an anti-HA antibody. Immunocomplexes were resolved on SDS-PAGE and immunoblotted with the indicated antibodies.

Detection of Notch1 ICN1 phosphorylation sites *in vitro* and *in vivo*

To map cyclin C-CDK8 phosphorylation sites on ICN1, *in vitro* kinase assays were performed as above. GST-ICN1 fusion protein-coupled beads were incubated with cyclin C-CDK8 recombinant complex (Invitrogen) in the presence of 0.2 mM cold ATP for 1 hr. Beads were washed three times with 50 μl of 50 mM Tris (pH 8.2). Beads were then resuspended in 50 μl of 50 mM Tris (pH 8.2) and digested with 0.5 μg of ASP-N overnight

at 37°C. The samples were then acidified using 50 μl of 1% formic acid and desalted using Stage-tips.

To map ICN1 phosphorylation status *in vivo*, 293 cells were transfected with Myc-ICN1. 40 hrs after transfection, cells were treated with 10 μM MG132 for 10 hrs before collecting cell lysates for anti-Myc-immunoprecipitation. Myc immunoprecipitated beads were washed and treated as in *in vitro* experiment.

To gauge cyclin C-CDK8 phosphorylation of T-ALL patient-derived Notch1 mutants, the following peptides were synthesized (from NeoBioLab), corresponding to amino acids 2507 to 2521of Notch1: wild-type: N-EHPFLTPSPESPDQWFPK-C; P2513A: N-EHPFLT**A**SPESPDQWFPK-C (mutated residue bold and underlined); P2513L: N-EHPFLT**L**SPESPDQWFPK-C; P2513S: N-EHPFLT**S**SPESPDQWFPK-C; P2514F: N-EHPFLTP**F**PESPDQWFPK-C; P2515R: N-EHPFLTPS**R**ESPDQWFPK-C. 1 μg of peptides were used for *in vitro* kinase reactions as above.

In *in vitro* and *in vivo* Notch1 phosphorylation analyses, samples were resuspended in 10 μl of 1% formic acid; subsequently 2 μl was used for analysis by LC-MS/MS. For the synthesized Notch1 peptide experiments, samples were resuspended in 100 μl and 2 μl was used for LC-MS/MS analysis.

For *in vitro* and *in vivo* Notch1 phosphorylation analyses, mass spectrometry was performed using an LTQ-Orbitrap Elite hybrid or Q-exactive mass spectrometer (MS) (Thermo Fisher, San Jose, CA). The raw, mzXML and results files have been deposited to the ProteomeXchange with identifier PXD001237 with detailed MS methods. An in-house suite of software was used for peptide identifications using the Sequest algorithm. Sequest searches were performed using the target decoy strategy and identifications were filtered using 1% false discovery rate using a linear discriminant analysis. More detailed methods can be found accompanied with the ProteomeXchange submission above.

CGH and gene expression array

Microarray-based comparative genomic hybridization (array CGH) was performed using Human Genome CGH 244A microarrays (Agilent Technologies, Santa Clara, CA) on T-ALL diagnostic specimens collected with informed consent and institutional board review approval from 47 children with T-ALL treated on clinical trials Children's Oncology Group P9404 or Dana-Farber Cancer Institute 00-01 (ref. 64, 65), as described[66]. Array CGH analysis of human T-ALL cell lines was performed using Human Genome CGH 44A microarrays (Agilent Technologies, Santa Clara, CA). Another set contained 94 cases of childhood ALL as described[67].

Gene expression microarrays were performed on 40 of the primary T-ALL patient samples analyzed by array CGH (shown in Fig. 7c), using Affymetrix U133 Plus 2.0 arrays, as described[65,66]. Cyclin C expression is from probe set 201955_at, CDK19 expression is from probe set 212897_at.

For analyses shown in Fig. 2d,e Affymetrix gene expression microarray data was normalized using RMA[68]. The log of the normalized gene expression data was then plotted.

Sequencing of *CCNC* in T-ALL patients

The full coding sequence of cyclin C (CCNC, CCDS34502, NM_005190) was sequenced by PCR amplification and Sanger sequencing, using genomic DNA from all primary T-ALL patient samples analyzed by array CGH that had sufficient DNA available (n = 43 of 47 in Fig. 7a). Sequencing was performed at Genewiz Inc., South Plainfield, NJ. Another set contained 104 cases of childhood ALL as described[67]. The sequencing was done by Beckman Coulter Genomics, Danvers, MA.

Sequencing of *Notch1* gene in T-ALL patients

Mutational screening of the LNR, HD-N, HD-C, TAD and PEST domains of *Notch1* was performed by denaturing high performance liquid chromatography and Sanger sequencing from diagnostic bone marrow samples from 73 patients with T-ALL (55 adult, 6 adolescent, and 12 pediatric) as previously described[51,69]. Patient characteristics have been reported[51,69,70]. Ethical approval for the trials and tissue collection for research was obtained from the Multi-Centre Research Ethics Committees and local research ethics committees as appropriate and informed consent was provided according to the Declaration of Helsinki.

Statistical analyses

The data was analyzed using two-tailed t-test, Log-rank test or Mann-Whitney test, as indicated. The data had normal distribution and the variance was similar between the groups being statistically compared. All western blotting or histological analyses have been repeated at least 3 times.

Accession numbers

Array CGH data are available on the NCBI Gene Expression Omnibus (GEO) website under accession numbers GSE14959 and GSE7615, gene expression data in T-ALL under accession number GSE14618, microarray data of cyclin C-null cells under accession number GSE58712. Mass spectrometry raw, mzXML and results files have been deposited to the ProteomeXchange with identifier PXD001237 along with detailed methods.

Supplementary Material

Refer to Web version on PubMed Central for supplementary material.

Acknowledgments

REFERENCES

1. Leopold P, O'Farrell PH. An evolutionarily conserved cyclin homolog from Drosophila rescues yeast deficient in G1 cyclins. Cell. 1991; 66:1207–16. [PubMed: 1833067]

2. Lew DJ, Dulic V, Reed SI. Isolation of three novel human cyclins by rescue of G1 cyclin (Cln) function in yeast. Cell. 1991; 66:1197–206. [PubMed: 1833066]

3. Malumbres M, Barbacid M. Cell cycle, CDKs and cancer: a changing paradigm. Nat Rev Cancer. 2009; 9:153–66. [PubMed: 19238148]

4. Liu ZJ, et al. A critical role for cyclin C in promotion of the hematopoietic cell cycle by cooperation with c-Myc. Mol Cell Biol. 1998; 18:3445–54. [PubMed: 9584184]

5. Makkonen KM, Malinen M, Ropponen A, Vaisanen S, Carlberg C. Cell cycle regulatory effects of retinoic Acid and forskolin are mediated by the cyclin C gene. J Mol Biol. 2009; 393:261–71. [PubMed: 19683536]

6. Miyata Y, et al. Cyclin C regulates human hematopoietic stem/progenitor cell quiescence. Stem Cells. 2010; 28:308–17. [PubMed: 19967789]

7. Ren S, Rollins BJ. Cyclin C/cdk3 promotes Rb-dependent G0 exit. Cell. 2004; 117:239–51. [PubMed: 15084261]

8. Saxena UH, et al. Phosphorylation by cyclin C/cyclin-dependent kinase 2 following mitogenic stimulation of murine fibroblasts inhibits transcriptional activity of LSF during G1 progression. Mol Cell Biol. 2009; 29:2335–45. [PubMed: 19237534]

9. Hengartner CJ, et al. Temporal regulation of RNA polymerase II by Srb10 and Kin28 cyclin-dependent kinases. Mol Cell. 1998; 2:43–53. [PubMed: 9702190]

10. Leclerc V, Tassan JP, O'Farrell PH, Nigg EA, Leopold P. Drosophila Cdk8, a kinase partner of cyclin C that interacts with the large subunit of RNA polymerase II. Mol Biol Cell. 1996; 7:505–13. [PubMed: 8730095]

11. Liao SM, et al. A kinase-cyclin pair in the RNA polymerase II holoenzyme. Nature. 1995; 374:193–6. [PubMed: 7877695]

12. Maldonado E, et al. A human RNA polymerase II complex associated with SRB and DNA-repair proteins. Nature. 1996; 381:86–9. [PubMed: 8609996]

13. Rickert P, Seghezzi W, Shanahan F, Cho H, Lees E. Cyclin C/CDK8 is a novel CTD kinase associated with RNA polymerase II. Oncogene. 1996; 12:2631–40. [PubMed: 8700522]

14. Tassan JP, Jaquenoud M, Leopold P, Schultz SJ, Nigg EA. Identification of human cyclin-dependent kinase 8, a putative protein kinase partner for cyclin C. Proc Natl Acad Sci U S A. 1995; 92:8871–5. [PubMed: 7568034]

15. Akoulitchev S, Chuikov S, Reinberg D. TFIIH is negatively regulated by cdk8-containing mediator complexes. Nature. 2000; 407:102–6. [PubMed: 10993082]

16. Elmlund H, et al. The cyclin-dependent kinase 8 module sterically blocks Mediator interactions with RNA polymerase II. Proc Natl Acad Sci U S A. 2006; 103:15788–93. [PubMed: 17043218]

17. Knuesel MT, Meyer KD, Bernecky C, Taatjes DJ. The human CDK8 subcomplex is a molecular switch that controls Mediator coactivator function. Genes Dev. 2009; 23:439–51. [PubMed: 19240132]

18. Alarcon C, et al. Nuclear CDKs drive Smad transcriptional activation and turnover in BMP and TGF-beta pathways. Cell. 2009; 139:757–69. [PubMed: 19914168]

19. Chi Y, et al. Negative regulation of Gcn4 and Msn2 transcription factors by Srb10 cyclin-dependent kinase. Genes Dev. 2001; 15:1078–92. [PubMed: 11331604]

20. Fryer CJ, White JB, Jones KA. Mastermind recruits CycC:CDK8 to phosphorylate the Notch ICD and coordinate activation with turnover. Mol Cell. 2004; 16:509–20. [PubMed: 15546612]

21. Nelson C, Goto S, Lund K, Hung W, Sadowski I. Srb10/Cdk8 regulates yeast filamentous growth by phosphorylating the transcription factor Ste12. Nature. 2003; 421:187–90. [PubMed: 12520306]

22. Donner AJ, Szostek S, Hoover JM, Espinosa JM. CDK8 is a stimulus-specific positive coregulator of p53 target genes. Mol Cell. 2007; 27:121–33. [PubMed: 17612495]

23. Firestein R, et al. CDK8 is a colorectal cancer oncogene that regulates beta-catenin activity. Nature. 2008; 455:547–51. [PubMed: 18794900]

24. Morris EJ, et al. E2F1 represses beta-catenin transcription and is antagonized by both pRB and CDK8. Nature. 2008; 455:552–6. [PubMed: 18794899]

25. Donner AJ, Ebmeier CC, Taatjes DJ, Espinosa JM. CDK8 is a positive regulator of transcriptional elongation within the serum response network. Nat Struct Mol Biol. 2010; 17:194–201. [PubMed: 20098423]

26. Furumoto T, et al. A kinase subunit of the human mediator complex, CDK8, positively regulates transcriptional activation. Genes Cells. 2007; 12:119–32. [PubMed: 17212659]

27. Li H, et al. Molecular cloning and chromosomal localization of the human cyclin C (CCNC) and cyclin E (CCNE) genes: deletion of the CCNC gene in human tumors. Genomics. 1996; 32:253–9. [PubMed: 8833152]

28. Ohata N, et al. Highly frequent allelic loss of chromosome 6q16-23 in osteosarcoma: involvement of cyclin C in osteosarcoma. Int J Mol Med. 2006; 18:1153–8. [PubMed: 17089020]

29. Bondi J, et al. Expression and gene amplification of primary (A, B1, D1, D3, and E) and secondary (C and H) cyclins in colon adenocarcinomas and correlation with patient outcome. J Clin Pathol. 2005; 58:509–14. [PubMed: 15858123]

30. Galamb O, et al. Evaluation of malignant and benign gastric biopsy specimens by mRNA expression profile and multivariate statistical methods. Cytometry B Clin Cytom. 2007; 72:299–309. [PubMed: 17366642]

31. Husdal A, Bukholm G, Bukholm IR. The prognostic value and overexpression of cyclin A is correlated with gene amplification of both cyclin A and cyclin E in breast cancer patient. Cell Oncol. 2006; 28:107–16. [PubMed: 16823179]

32. Iqbal J, et al. Clinical implication of genome-wide profiling in diffuse large B-cell lymphoma and other subtypes of B-cell lymphoma. Indian J Cancer. 2007; 44:72–86. [PubMed: 17938484]

33. Xu W, Ji JY. Dysregulation of CDK8 and Cyclin C in tumorigenesis. J Genet Genomics. 2011; 38:439–52. [PubMed: 22035865]

34. Tronche F, et al. Disruption of the glucocorticoid receptor gene in the nervous system results in reduced anxiety. Nat Genet. 1999; 23:99–103. [PubMed: 10471508]

35. Ye X, Zhu C, Harper JW. A premature-termination mutation in the Mus musculus cyclin-dependent kinase 3 gene. Proc Natl Acad Sci U S A. 2001; 98:1682–6. [PubMed: 11172011]

36. Kuhn R, Schwenk F, Aguet M, Rajewsky K. Inducible gene targeting in mice. Science. 1995; 269:1427–9. [PubMed: 7660125]

37. Malumbres M. Physiological relevance of cell cycle kinases. Physiol Rev. 2011; 91:973–1007. [PubMed: 21742793]

38. Welcker M, Clurman BE. FBW7 ubiquitin ligase: a tumour suppressor at the crossroads of cell division, growth and differentiation. Nat Rev Cancer. 2008; 8:83–93. [PubMed: 18094723]

39. Weng AP, et al. Activating mutations of NOTCH1 in human T cell acute lymphoblastic leukemia. Science. 2004; 306:269–71. [PubMed: 15472075]

40. Thompson BJ, et al. The SCFFBW7 ubiquitin ligase complex as a tumor suppressor in T cell leukemia. J Exp Med. 2007; 204:1825–35. [PubMed: 17646408]

41. Chiang MY, et al. Leukemia-associated NOTCH1 alleles are weak tumor initiators but accelerate K-ras-initiated leukemia. J Clin Invest. 2008; 118:3181–94. [PubMed: 18677410]

42. Boehm T, Foroni L, Kaneko Y, Perutz MF, Rabbitts TH. The rhombotin family of cysteine-rich LIM-domain oncogenes: distinct members are involved in T-cell translocations to human chromosomes 11p15 and 11p13. Proc Natl Acad Sci U S A. 1991; 88:4367–71. [PubMed: 2034676]

43. Larson RC, et al. T cell tumours of disparate phenotype in mice transgenic for Rbtn-2. Oncogene. 1994; 9:3675–81. [PubMed: 7970726]

44. McGuire EA, Rintoul CE, Sclar GM, Korsmeyer SJ. Thymic overexpression of Ttg-1 in transgenic mice results in T-cell acute lymphoblastic leukemia/lymphoma. Mol Cell Biol. 1992; 12:4186–96. [PubMed: 1508213]

45. Lin YW, Nichols RA, Letterio JJ, Aplan PD. Notch1 mutations are important for leukemic transformation in murine models of precursor-T leukemia/lymphoma. Blood. 2006; 107:2540–3. [PubMed: 16282337]

46. O'Neil J, et al. Activating Notch1 mutations in mouse models of T-ALL. Blood. 2006; 107:781–5. [PubMed: 16166587]

47. Hyytinen ER, et al. Defining the region(s) of deletion at 6q16-q22 in human prostate cancer. Genes Chromosomes Cancer. 2002; 34:306–12. [PubMed: 12007191]

48. Orphanos V, et al. Allelic imbalance of chromosome 6q in ovarian tumours. Br J Cancer. 1995; 71:666–9. [PubMed: 7710926]

49. Utada Y, et al. Mapping of target regions of allelic loss in primary breast cancers to 1-cM intervals on genomic contigs at 6q21 and 6q25.3. Jpn J Cancer Res. 2000; 91:293–300. [PubMed: 10760688]

50. Zhang Y, et al. A 3-cM commonly deleted region in 6q21 in leukemias and lymphomas delineated by fluorescence in situ hybridization. Genes Chromosomes Cancer. 2000; 27:52–8. [PubMed: 10564586]

51. Mansour MR, et al. Prognostic implications of NOTCH1 and FBXW7 mutations in adults with T-cell acute lymphoblastic leukemia treated on the MRC UKALLXII/ECOG E2993 protocol. J Clin Oncol. 2009; 27:4352–6. [PubMed: 19635999]

52. Koch U, Radtke F. Notch signaling in solid tumors. Curr Top Dev Biol. 2010; 92:411–55. [PubMed: 20816403]

53. Jackson A, et al. Deletion of 6q16-q21 in human lymphoid malignancies: a mapping and deletion analysis. Cancer Res. 2000; 60:2775–9. [PubMed: 10850412]

54. Sinclair PB, et al. A fluorescence in situ hybridization map of 6q deletions in acute lymphocytic leukemia: identification and analysis of a candidate tumor suppressor gene. Cancer Res. 2004; 64:4089–98. [PubMed: 15205317]

55. Lobry C, Oh P, Mansour MR, Look AT, Aifantis I. Notch signaling: switching an oncogene to a tumor suppressor. Blood. 2014; 123:2451–9. [PubMed: 24608975]

56. Agrawal N, et al. Exome sequencing of head and neck squamous cell carcinoma reveals inactivating mutations in NOTCH1. Science. 2011; 333:1154–7. [PubMed: 21798897]

57. Nicolas M, et al. Notch1 functions as a tumor suppressor in mouse skin. Nat Genet. 2003; 33:416–21. [PubMed: 12590261]

58. Stransky N, et al. The mutational landscape of head and neck squamous cell carcinoma. Science. 2011; 333:1157–60. [PubMed: 21798893]

59. King B, et al. The ubiquitin ligase FBXW7 modulates leukemia-initiating cell activity by regulating MYC stability. Cell. 2013; 153:1552–66. [PubMed: 23791182]

60. Li X, Gounari F, Protopopov A, Khazaie K, von Boehmer H. Oncogenesis of T-ALL and nonmalignant consequences of overexpressing intracellular NOTCH1. J Exp Med. 2008; 205:2851–61. [PubMed: 18981238]

61. Chiang MY, et al. Identification of a conserved negative regulatory sequence that influences the leukemogenic activity of NOTCH1. Mol Cell Biol. 2006; 26:6261–71. [PubMed: 16880534]

62. Inuzuka H, et al. Phosphorylation by casein kinase I promotes the turnover of the Mdm2 oncoprotein via the SCF(beta-TRCP) ubiquitin ligase. Cancer Cell. 2010; 18:147–59. [PubMed: 20708156]

63. Emmerich CH, et al. Activation of the canonical IKK complex by K63/M1-linked hybrid ubiquitin chains. Proc Natl Acad Sci U S A. 2013; 110:15247–52. [PubMed: 23986494]

64. Vrooman LM, et al. Postinduction dexamethasone and individualized dosing of Escherichia Coli L-asparaginase each improve outcome of children and adolescents with newly diagnosed acute lymphoblastic leukemia: results from a randomized study--Dana-Farber Cancer Institute ALL Consortium Protocol 00-01. J Clin Oncol. 2013; 31:1202–10. [PubMed: 23358966]

65. Winter SS, et al. Identification of genomic classifiers that distinguish induction failure in T-lineage acute lymphoblastic leukemia: a report from the Children's Oncology Group. Blood. 2007; 110:1429–38. [PubMed: 17495134]

66. Gutierrez A, et al. Inactivation of LEF1 in T-cell acute lymphoblastic leukemia. Blood. 2010; 115:2845–51. [PubMed: 20124220]

67. Zhang J, et al. The genetic basis of early T-cell precursor acute lymphoblastic leukaemia. Nature. 2012; 481:157–63. [PubMed: 22237106]

68. Irizarry RA, et al. Exploration, normalization, and summaries of high density oligonucleotide array probe level data. Biostatistics. 2003; 4:249–64. [PubMed: 12925520]

69. Mansour MR, et al. Notch-1 mutations are secondary events in some patients with T-cell acute lymphoblastic leukemia. Clin Cancer Res. 2007; 13:6964–9. [PubMed: 18056171]

70. Mansour MR, Linch DC, Foroni L, Goldstone AH, Gale RE. High incidence of Notch-1 mutations in adult patients with T-cell acute lymphoblastic leukemia. Leukemia. 2006; 20:537–9. [PubMed: 16424867]
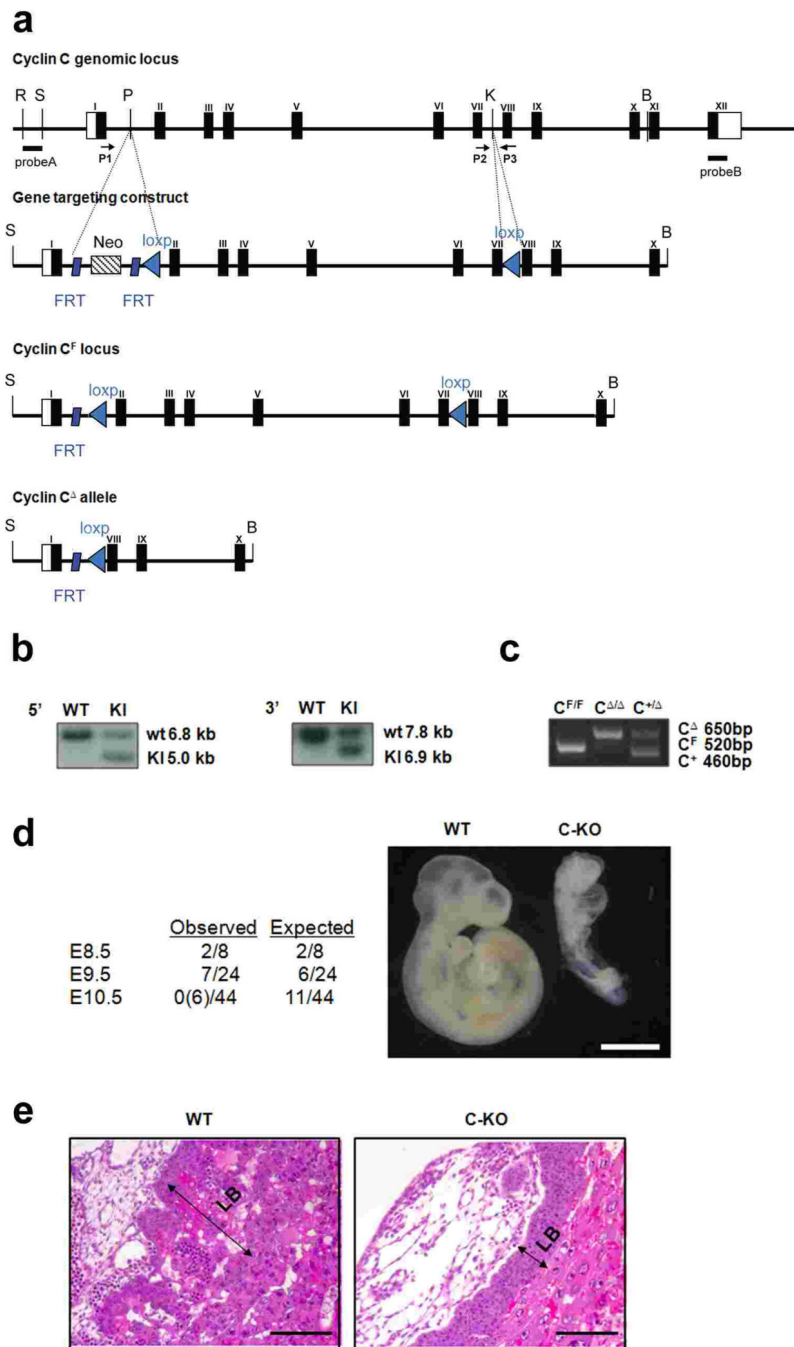
Figure 1.
Generation and analyses of cyclin C knockout mice. (**a**) Cyclin C gene targeting strategy. Coding exons are shown as filled boxes. Neo, *neomycin phosphotransferase* gene; loxP and FRT sequences are indicated as light blue triangles and dark blue rectangles, respectively. Restriction enzymes recognition sites: B, BMgBI; K, KpnI; P, PvuII; R, EcoRI; S, SalI. Solid black lines represent Southern blotting probes A and B used to screen for homologous recombination. Arrows show PCR primers (P1, P2, P3) used for genotyping the animals. (**b**) Southern blot analysis of genomic DNA extracted from wild-type (WT) and cyclin C$^{+/F(Neo)}$

(KI) ES cell clones. DNA was digested with EcoRI and hybridized with probe A (5' end screening) or probe B (3' end screening). The sizes of WT and recombinant alleles are shown. (**c**) PCR analysis of cyclin $C^{F/F}$, $C^{-/-}$ and $C^{+/-}$ mice. The sizes of PCR products from the wild-type (C^+), "floxed" (C^F) and deleted (C^-) alleles are marked. (**d**) Left panel: the proportion of observed live cyclin $C^{-/-}$ embryos among all embryos at the indicated days of embryonic development (E8.5-10.5). Numbers in brackets denote dead embryos. The expected Mendelian proportion of cyclin $C^{-/-}$ embryos is also presented. Right panel: the photograph shows microscopic images of wild-type (WT) and cyclin $C^{-/-}$ (C-KO) littermates at E9.5. Scale bar, 0.5 mm. The absence of full-length cyclin C transcript in cyclin $C^{-/-}$ embryo was verified by RT-PCR. (**e**) Microscopic appearance of placentas from wild-type and cyclin $C^{-/-}$ (C-KO) embryos at E9.5. Histologic sections were stained with hematoxylin and eosin. Note underdeveloped labirynth layer (LB) in cyclin C-KO placenta. Scale bars, 50 μm.
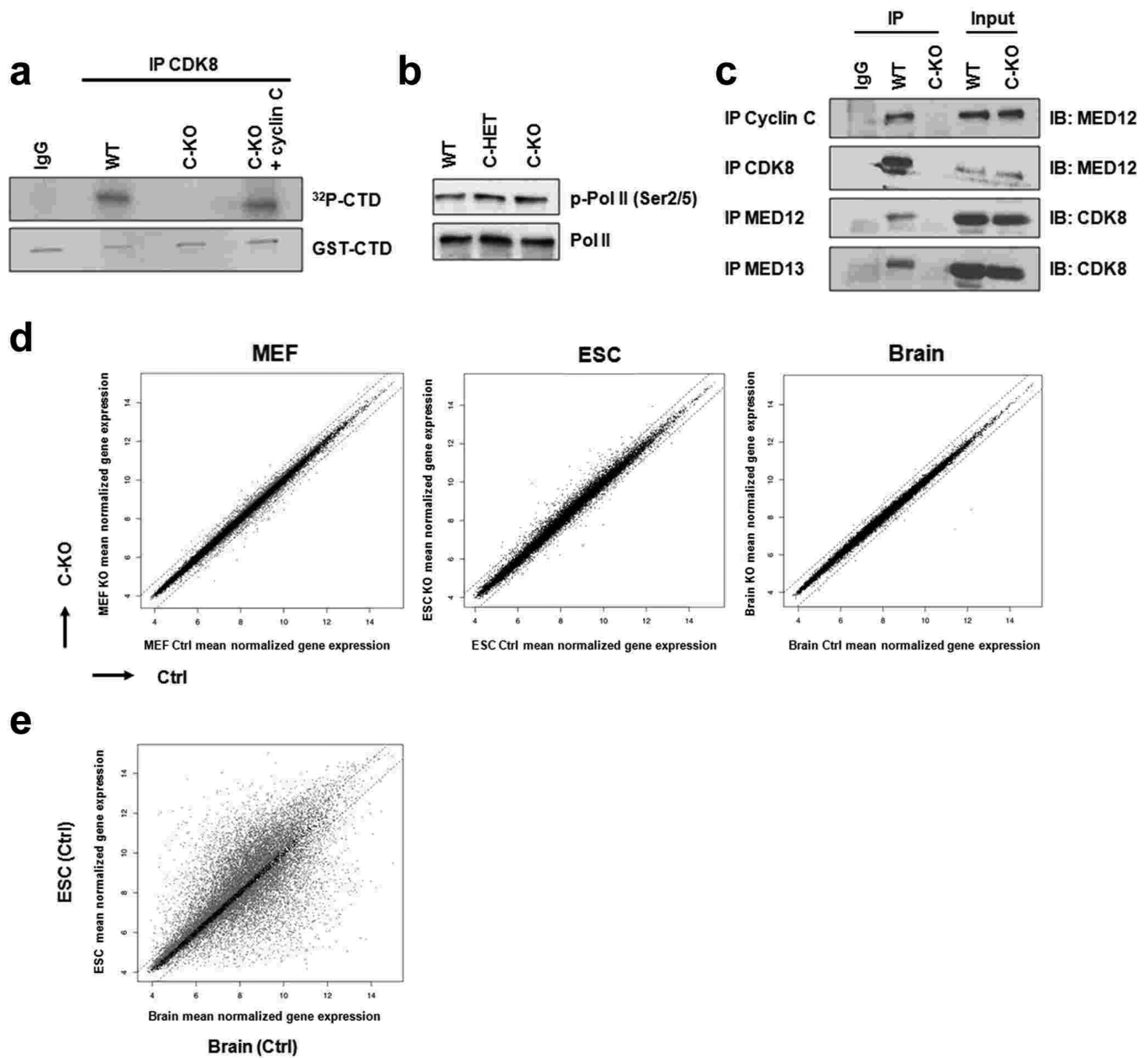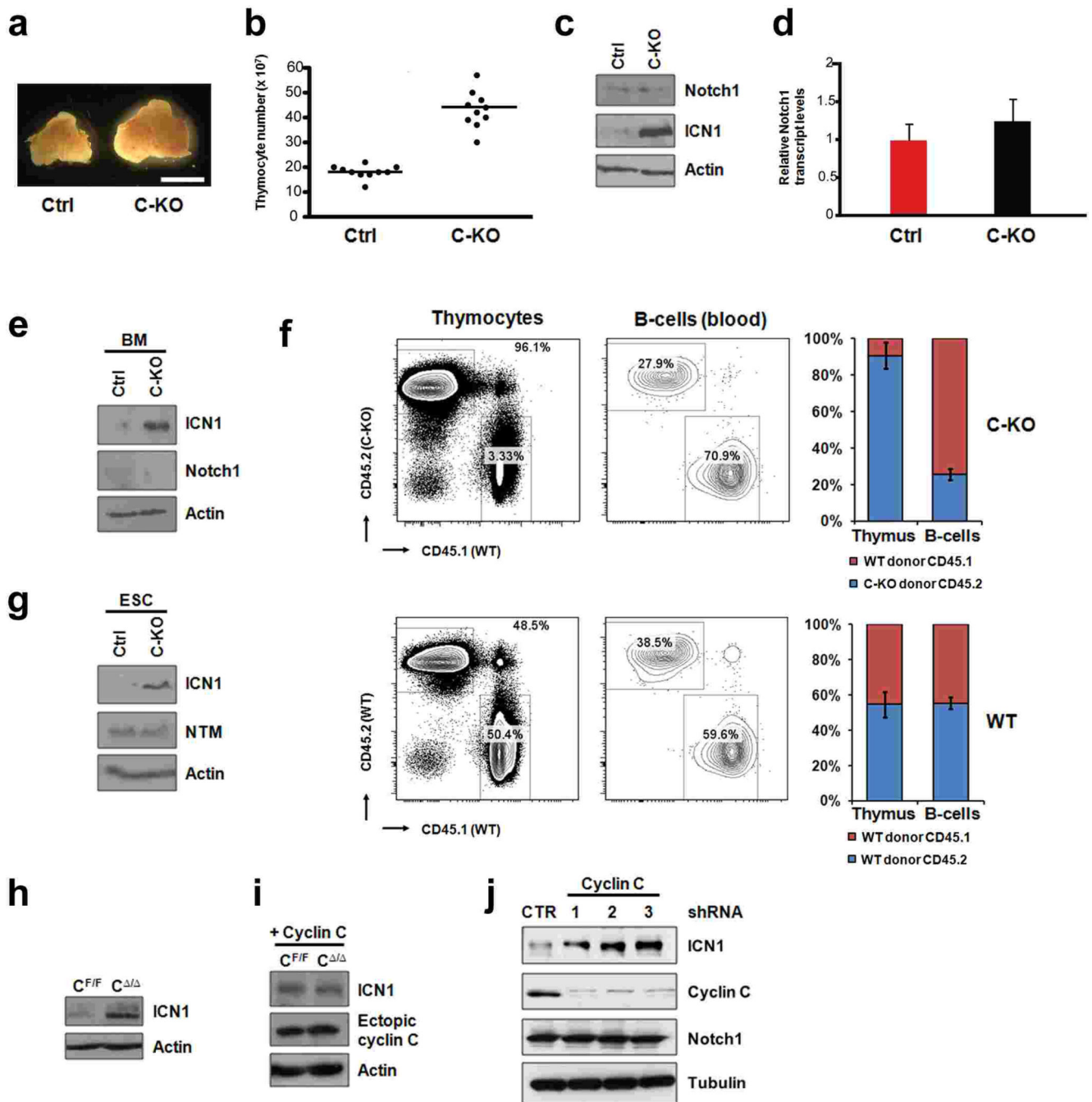
Figure 2.
Gene expression analyses of cyclin C-null cells. (**a**) CDK8 was immunoprecipitated (IP) from wild-type (WT) or cyclin C $^{/}$ (C-KO) MEFs and used for *in vitro* kinase reactions with recombinant carboxy terminal domain (CTD) of RNA polymerase II as a substrate, in the presence of γ[^{32}P]ATP. C-KO + cyclin C: cyclin C $^{/}$ MEFs engineered to ectopically express cyclin C. Note that re-expression of cyclin C restored CDK8 kinase activity in cyclin C $^{/}$ cells. IgG was used for control immunoprecipitation. ^{32}P-CTD denotes phosphorylated CTD, detected by autoradiography. Lower panel, CTD was visualized by Coomassie staining. (**b**) Lysates from wild-type (WT), cyclin C$^{+/}$ (C-HET) and cyclin C $^{/}$ (C-KO) ES cells were probed with an antibody against phospho-Ser 2 and phospho-Ser 5 of RNA polymerase II CTD. Lower panel: immunoblotting with an anti-CTD antibody. (**c**)

Cyclin C, CDK8, MED12 or MED13 were immunoprecipitated (IP) from wild-type or C-KO MEFs; the immunoblots were probed with the indicated antibodies, along with whole cell extracts (Input). (**d**) Scatterplot showing log of the normalized gene expression in control (x-axis) vs. C $^{/}$ (y-axis) MEFs, ES cells (ESC) and E18.5 brains. Parallel lines indicate 2-fold change (up- or down-regulation) in transcript levels. (**e**) Scatterplot showing log of the normalized gene expression values in control brains (x-axis) vs. control ES cells (y-axis). This is a control to panel **d**. It illustrates that different compartments (brain, ES cells) display very distinct gene expression patterns, as expected.
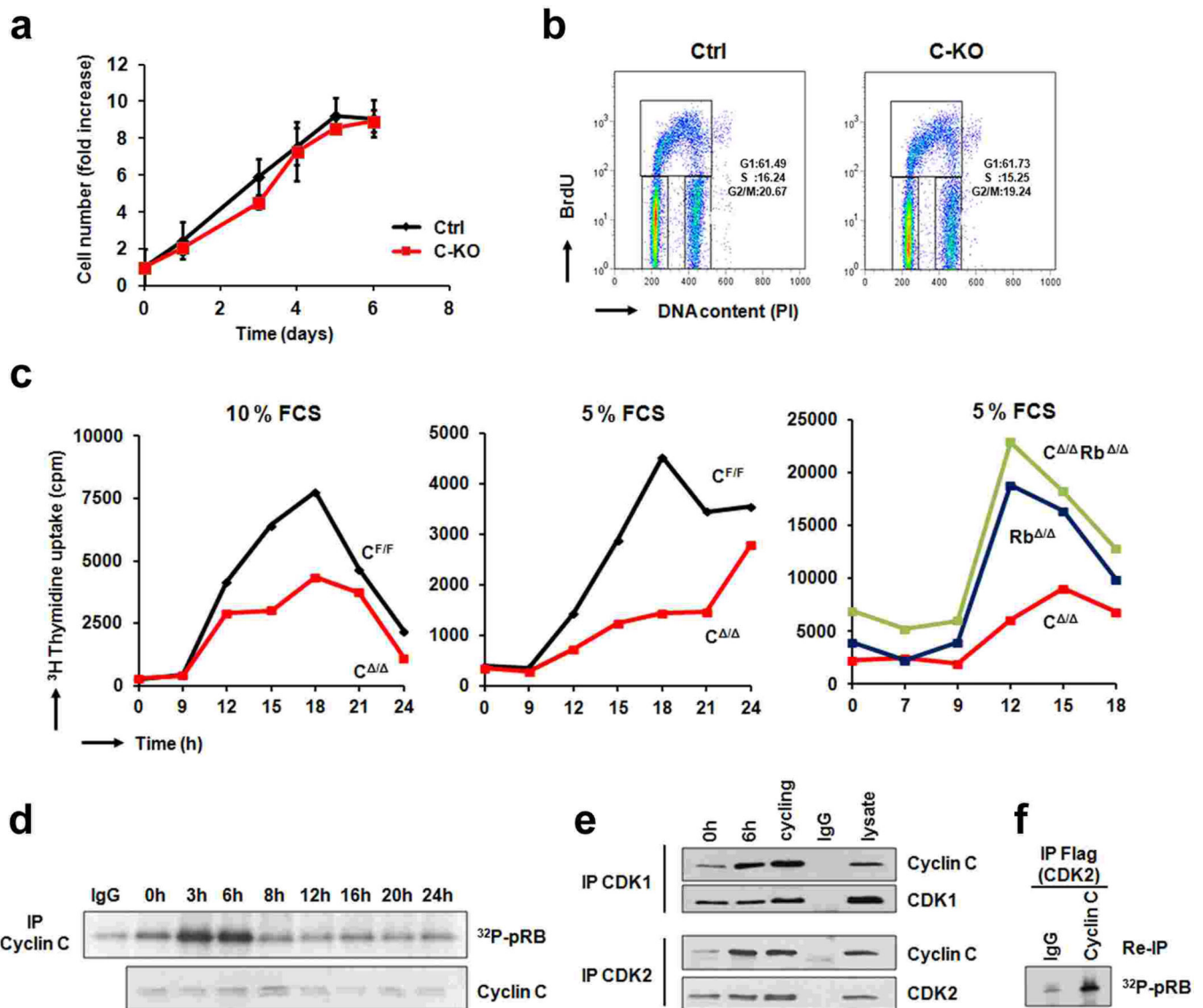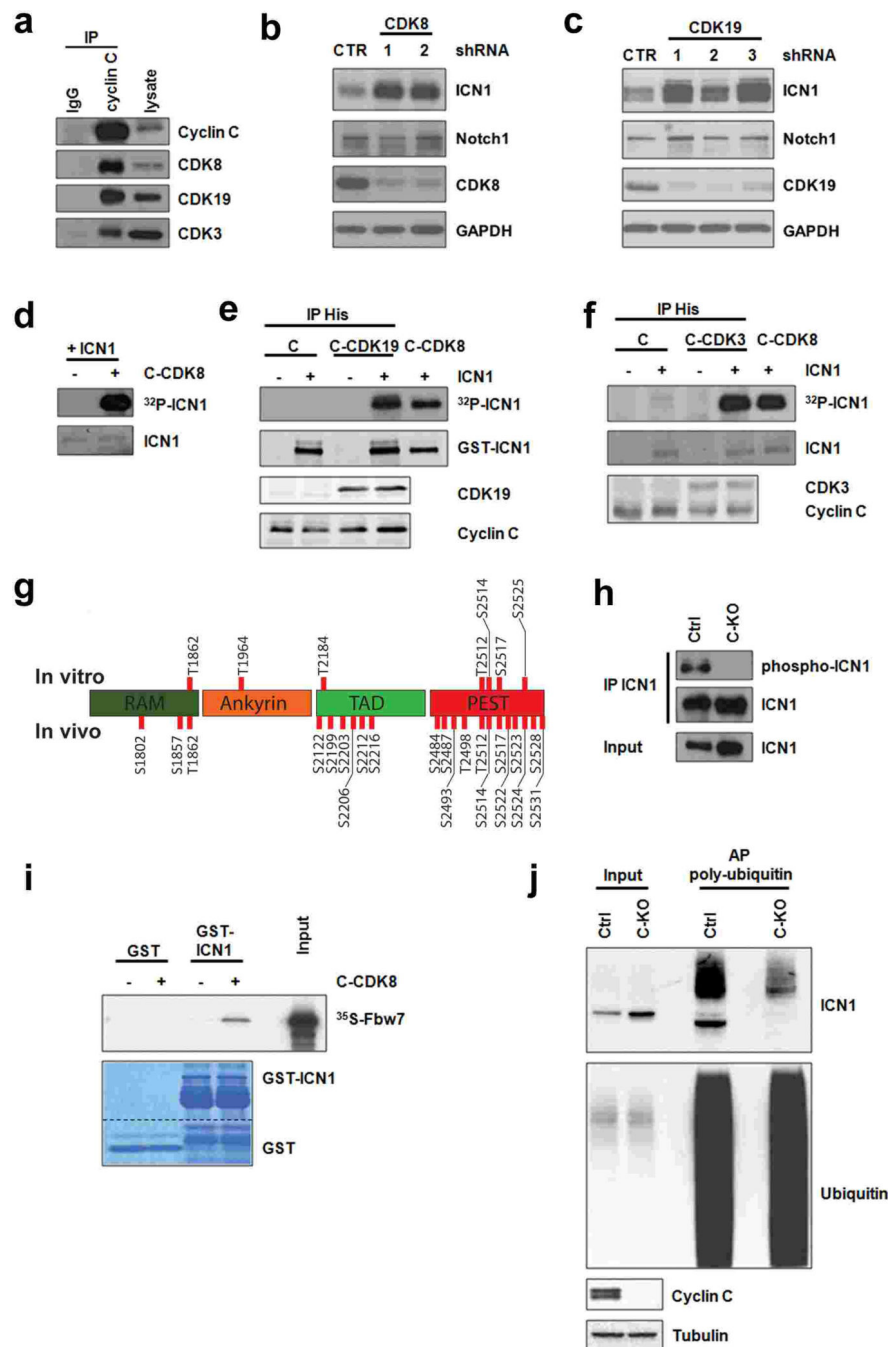
Figure 3.

Cell cycle analyses of cyclin C-null cells. (**a**) *In vitro* growth-curves of cyclin $C^{F/F}$ (Ctrl) and $C^{\Delta/\Delta}$ (C-KO) MEFs, n=3. P=0.8 (day 4), P=0.8 (day 5), P=0.7 (day 6, all using t-test). (**b**) Fraction of cyclin $C^{F/F}$ (Ctrl) and $C^{\Delta/\Delta}$ (C-KO) MEFs in different cell cycle phases, visualized by propidium iodide (DNA content) and anti-BrdU staining followed by FACS. (**c**) MEFs were rendered quiescent by serum starvation, and then stimulated to re-enter the cell cycle from G_0 by addition of medium containing the indicated concentrations of serum (FCS). Entry of cells into the S-phase was evaluated by measuring [^{3}H]-thymidine uptake. Left panel: P=0.003 (at 18 hrs); middle panel: P=0.028 (at 18 hrs); right panel: P=0.007 ($C^{\Delta/\Delta}$ vs. $C^{\Delta/\Delta}$ $Rb^{\Delta/\Delta}$), P=0.202 ($Rb^{\Delta/\Delta}$ vs. $C^{\Delta/\Delta}$ $Rb^{\Delta/\Delta}$), both at 12 hrs. P values were determined by t-test. (**d**) Wild-type MEFs were arrested in G_0 as above, and then stimulated to re-enter the cell cycle by addition of medium containing 10% serum. Upper panel: at the indicated time-points, cyclin C was immunoprecipitated and used for *in vitro* kinase reactions with recombinant pRB as a substrate in the presence of γ[^{32}P]ATP. ^{32}P-pRB

denotes phosphorylated pRB, detected by autoradiography. Lower panel: the levels of cyclin C at the indicated time-points were determined by western blotting. (**e**) CDK1 or CDK2 were immunoprecipitated from quiescent MEFs (0h), or at 6 hrs after serum stimulation, or from asynchronously growing cells (Cycling). Immunoblots were probed with the indicated antibodies. Lysate, denotes straight lysate from cycling cells. (**f**) Flag-tagged CDK2 was expressed in 293T cells and immunoprecipitated (IP) with an anti-Flag antibody. Complexes were eluted with a Flag peptide, re-immunoprecipitated (re-IP) with an anti-cyclin C antibody (or, for control with IgG), and used for *in vitro* kinase reactions with recombinant pRB as a substrate. ^{32}P-pRB denotes phosphorylated pRB, detected by autoradiography.

Figure 4.
Genetic ablation of cyclin C upregulates ICN1. (**a**) Appearance of thymuses from 6-weeks-old control ($C^{F/F}$/Mx1-Cre$^-$) and C $^{/}$ /Mx1-Cre (C-KO) mice. Scale bar, 4 mm. (**b**) Total number of thymocytes in 4-6 weeks-old control (n=10) and C-KO mice (n=10). Horizontal lines denote mean values. *P*<0.001 (t-test). (**c**) Western blot analysis of thymocytes from control and C-KO mice (genotypes as in **a**). Immunoblots were probed with an antibody against full-length Notch1 (Notch1) or intracellular Notch1 (ICN1). (**d**) RT-PCR analysis of Notch1 mRNA levels in thymocytes from control (n=5) or C-KO mice (n=5); genotypes as

in **a**. Bars denote mean values, error bars, SD. *P*=0.25 (t-test). (**e**) Western blot analysis of bone marrow cells (BM) from control and C-KO mice, probed as in **c**. (**f**) Lethally irradiated CD45.1 wild-type (WT) mice were co-transferred with T-cell-depleted bone marrow from CD45.1 WT and CD45.2 cyclin $C^{/}$ (C-KO, upper row) or from CD45.1 WT and CD45.2 WT mice (WT, lower row). Subsequently, thymocytes and peripheral blood leukocytes of the bone marrow chimeras were stained for CD45.1, CD45.2 and CD19 (blood cells only) and analyzed by FACS. Expression of CD45.1 and CD45.2 in total thymocytes and blood B-cells (CD19$^+$) is presented as representative FACS plots and bar histograms of mean values. Error bars, SD (n=4 for WT:C-KO, and n = 3 for WT:WT chimeras). *P*<0.001 for C-KO thymus vs. C-KO B-cells; *P*= 0.91 for WT thymus vs. WT B-cells (t-test). (**g**) Western blot analysis of control and $C^{/}$ ES cells (ESC) probed with antibodies against ICN1 and membrane-bound, cleaved Notch1 (NTM). (**h**) Cyclin $C^{F/F}$ MEFs were transduced with a virus encoding Notch1. Cells were then treated with a control adenovirus ($C^{F/F}$), or with Cre-expressing adenovirus, leading to ablation of cyclin C ($C^{/}$). The levels of ICN1 were determined by immunoblotting. (**i**) Similar experiment as in **h**, except that cells were transduced with a virus encoding cyclin C (+cyclin C) prior to deletion of the endogenous cyclin C. The levels of ectopically expressed cyclin C (Ectopic cyclin C) were determined by immunoblotting. (**j**) Human T-ALL MOLT-16 cells were transduced with viruses expressing three different anti-cyclin C shRNAs (1, 2 or 3), or control shRNA (CTR). Cells were harvested and lysates probed with the indicated antibodies.

Figure 5.
Phosphorylation of ICN1 by cyclin C-CDK8, C-CDK19 and C-CDK3 kinases. (**a**) Cyclin C was immunoprecipitated (IP) from MOLT-16 cells, immunoblots were probed with the indicated antibodies. Lysate, whole cell extracts. (**b**) Cyclin C$^{F/F}$ MEFs stably expressing ICN1 were transduced with two anti-CDK8 shRNAs (1 or 2) or with control shRNA (CTR). Cell extracts were imunoblotted with the indicated antibodies. Notch1, antibody against full-length Notch1. (**c**) Similar analysis as in **b**, using anti-CDK19 shRNAs (1, 2 or 3). (**d**), Purified, recombinant ICN1 was incubated in the presence (+) or absence (−) of recombinant

cyclin C-CDK8 with γ[^{32}P]ATP. Upper panel: proteins analyzed by autoradiography, ^{32}P-ICN1 denotes phosphorylated ICN1. Lower panel: ICN1 visualized by Ponceau S staining. (**e**) His-tagged cyclin C or cyclin C and CDK19 were expressed in Sf9 cells, purified using anti-His antibodies, and used for *in vitro* kinase reactions in the presence (+) or absence (−) of ICN1 as a substrate with γ[^{32}P]ATP. As a positive control, ICN1 was incubated with recombinant cyclin C-CDK8. Upper panel: proteins analyzed by autoradiography to detect phosphorylated ICN1 (^{32}P-ICN1). Second panel: GST-ICN1 protein detected by immunoblotting with anti-GST antibody. Third and fourth panels: CDK19 and cyclin C detected using the indicated antibodies. (**f**) Similar analyses as in **e**, using cyclin C and CDK3. ICN1 protein was detected by Ponceau S staining. (**g**) A diagram of ICN1 protein used for phosphorylation analyses, with RAM (RBP-Jkappa-associated-module), Ankyrin repeat, transactivation domain (TAD) and PEST domains marked. Numbers above the ICN1 depict residues identified to be phosphorylated by cyclin C-CDK8 *in vitro*, numbers below show residues phosphorylated *in vivo*. (**h**) Protein extracts were prepared from thymocytes from C$^{F/F}$/Mx1-Cre$^{−}$ (Ctrl) and C$^{/}$/Mx1-Cre (C-KO) mice, ICN1 was immunoprecipitated (IP) and immunoblots probed with a phospho-specific antibody against Ser2517-phoshorylated ICN1 (phospho-ICN1), or with anti-ICN1 antibody. Input denotes whole cell extracts. (**i**) Purified recombinant GST-ICN1 was pre-incubated in the presence (+) or absence (−) of cyclin C-CDK8 kinase. Subsequently, GST-ICN1 was incubated with *in vitro* translated ^{35}S-labeled Fbw7. ICN1-bound proteins were visualized by autoradiography. GST beads were used as a negative control. Input: an aliquot of radiolabeled Fbw7. Note that ICN1 interacted with Fbw7 only after pre-incubation with cyclin C-CDK8. Lower panel: Coomassie stained gel. The middle portion of the gel was cut out and the images were spliced together (dashed line). (**j**) Protein extracts were prepared from thymocytes from Ctrl and C-KO mice (as in **h**). Polyubiquitinated proteins were captured with Halo-TUBE (AP, affinity purification poly-ubiquitin), and immunoblotted with the indicated antibodies. Input, cell extracts. Note reduced polyubiquitination of the endogenous ICN1 in C-KO thymocytes.
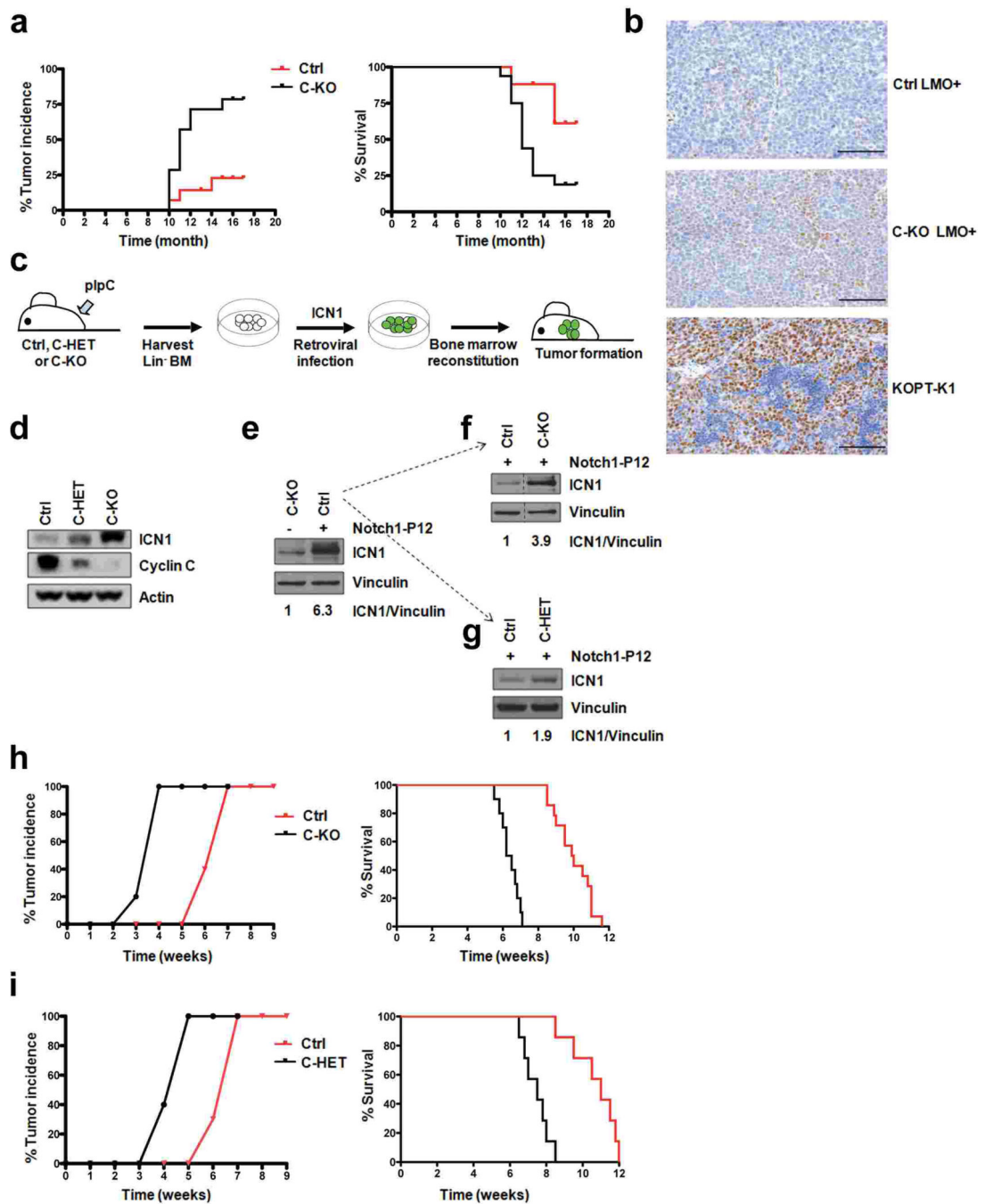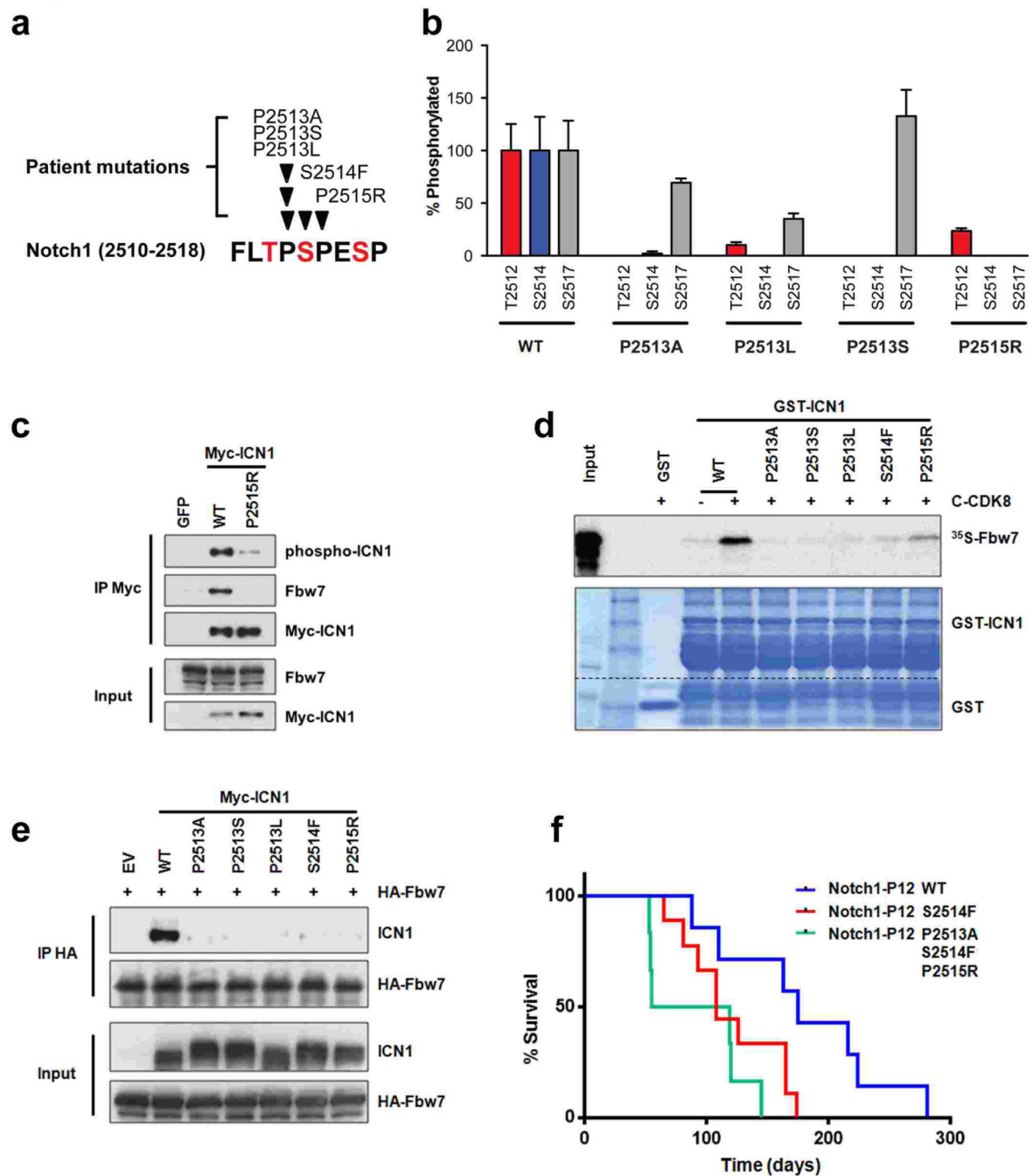
Figure 6.
Cyclin C is a haploinsufficient tumor suppressor. (**a**) Tumor incidence (left) and Kaplan-Meier survival analysis (right) in $C^{F/F}$/LMO1/Mx-Cre⁻ (Ctrl) and $C^{/}$/LMO1/Mx-Cre⁺ (C-KO) mice. N=14 per group. *P*=0.0023 (Log-rank test). (**b**) Tumor sections (genotypes as in **a**) were stained for ICN1. Note increased ICN1 levels in C-KO tumor. Human T-ALL KOPT-K1 cells were used as a positive control. Scale bar, 100μm (**c**) Schematic representation of the experimental design to trigger T-ALL in mice. $C^{F/F}$/Mx1-Cre⁻ (Ctrl), $C^{+/F}$/Mx1-Cre (C-HET), or $C^{F/F}$/Mx1-Cre (C-KO) animals were injected with poIy-polyC

(to delete cyclin C). Bone marrow was collected, HPC were sorted, and transduced with a retrovirus encoding ICN1 and GFP, or Notch1-P12 and GFP and injected into wild-type recipient mice. (**d**) HPC were isolated from pI-pC-treated $C^{F/F}$/Mx1-Cre$^-$ (Ctrl), $C^{+/}$ /Mx1-Cre (C-HET) and C $^/$ /Mx1-Cre (C-KO) animals and cultured for 48 h on OP9-DL1 stroma. The levels of ICN1 and cyclin C were detected by immunoblotting. Note increased endogenous ICN1 levels in C-HET and C-KO. (**e**) Comparison of ICN1 levels in non-manipulated HPC from C-KO mice (C-KO, −Notch1), vs. HPC from control mice transduced with oncogenic Notch1-P12 (Ctrl, +Notch1). Note strongly increased (>6-fold) ICN1 levels in cells expressing Notch1-P12. Hence, although cyclin C-KO HPC express elevated levels of endogenous ICN1 as compared to control HPC (panel **d**), this level is still substantially lower than the level of ectopically expressed ICN1 upon viral transduction (i.e., the level needed to trigger T-ALL). (**f**) Comparison of ICN1 levels in HPC of Ctrl vs. C-KO mice. Both genotypes were transduced with Notch1-P12. Note elevated (~4-fold) levels of ectopically expressed ICN1 in C-KO cells. The middle portion of the gel was cut out and the images were spliced together (dashed line). (**g**) Comparison of ICN1 levels in HPC of Ctrl vs. C-HET mice. Both genotypes were transduced with Notch1-P12. Note elevated (~2-fold) levels of ectopically expressed ICN1 in C-HET cells. In **e-g**, numbers below the gels denote densitometric quantification of ICN1 band densities (ImageJ). Dashed lines indicate that the lane 2 in panel **e**, lane 1 in panel **f**, and lane 1 in panel **g** show control HPC transduced with Notch1-P12. (**h**) Mice received ICN1-transduced $C^{F/F}$ (Ctrl) or C $^/$ (C-KO) HPC. Left: tumor incidence, n=20 per group. Right: Kaplan-Meier analysis of survival, n=14 in control, n=10 in cyclin C-KO. *P*<0.0001 (Log-rank test). (**i**) Mice received ICN1-transduced $C^{F/F}$ (Ctrl) or $C^{+/}$ (C-HET) HPC. Left: tumor incidence, n=10 per group. Right: Kaplan-Meier analysis of survival, n=7 per group. *P*=0.0003 (Log-rank test).
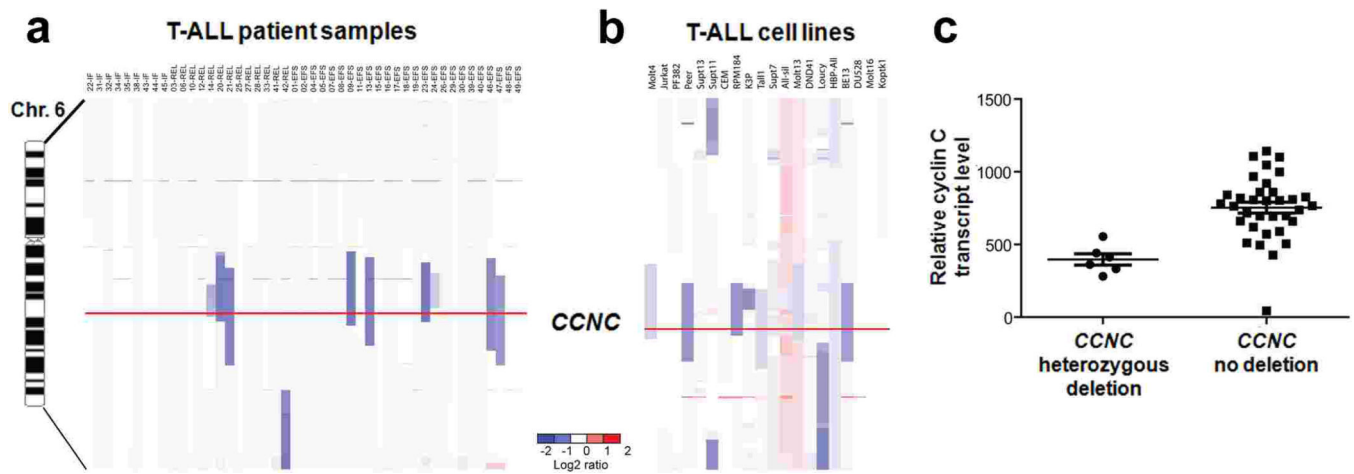
Figure 7.
Cyclin C is heterozygously deleted in human T-ALL. (**a**) Array CGH was performed on genomic DNA from primary T-ALL patient samples and (**b**) human T-ALL cell lines. Patient samples are grouped by clinical outcome (IF, induction failure; REL, relapse; EFS, long-term event-free survivor). Shown is a dChip plot of the segmented CGH log2 copy number ratios of the entire chromosome 6. Location of the *CCNC* locus is denoted by a red line. (**c**) Cyclin C expression was analyzed using gene expression microarrays; analysis was performed on a subset of primary T-ALL patient samples depicted in **a**. Shown are cyclin C expression levels in tumors which displayed heterozygous *CCNC* gene deletions (n=6) vs. tumors without *CCNC* deletion (*CCNC* no del, n=34). *P*=0.006 (Mann-Whitney test).

Figure 8.
T-ALL patient-derived mutations block the ability of cyclin C-CDK to phosphorylate critical ICN1 residues and are oncogenic *in vivo*. (**a**) Schematic representation of missense mutations found in T-ALL patients. ICN1 aminoacids shown in red represent critical cyclin C-CDK-dependent phosphoresidues on Notch1 (T2512, S2514, S2517). Arrowheads depict mutations found in T-ALL patients. All 5 patients had also mutations within Notch1 HD-domain. (**b**) Mass spectrometry quantitative analysis of ICN1 phosphorylation levels at three critical cyclin C-CDK8-dependent phosphoresidues. A peptide containing wild-type ICN1

sequence, or peptides with the indicated patient-derived aminoacid substitutions were incubated with cyclin C-CDK8 kinase, and stoichiometry of phosphorylation at T2512, S2514 and S2517 was quantified by mass spectrometry. The level of phosphorylation seen in ICN1 wild-type peptide was set at 100%. (**c**) Human T-ALL MOLT-4 cells were transduced with retroviruses expressing Myc-tagged wild-type ICN1 (WT) plus GFP, or ICN1 containing patient-derived P2515R mutation plus GFP, or GFP only. ICN1 was immunoprecipitated from GFP^{+} cells using anti-Myc antibody, immunoblots were probed with indicated antibodies. Phospho-ICN1 denotes anti-phospho-Ser2517-ICN1 antibody. (**d**) Purified, recombinant GST-tagged wild-type ICN1, or ICN1 mutants containing the indicated patient-derived aminoacid substitutions were pre-incubated with cyclin C-CDK8 kinase. Subsequently, GST-ICN1 was incubated with *in vitro* translated ^{35}S-labeled Fbw7. ICN1-bound Fbw7 was visualized by autoradiography. Input: an aliquot of radiolabeled Fbw7. Note that all patient-derived mutants were compromised in their ability to bind Fbw7. Lower panel: Coomassie-stained gel. The middle portion of the gel was cut out and images were spliced together (dashed line). (**e**) HeLa cells were transfected with an empty vector (EV), Myc-tagged wild-type ICN1 (WT) or ICN1 mutants containing the indicated patient-derived aminoacid substitutions, together with HA-tagged-Fbw7. Fbw7 was immunoprecipitated (IP HA), immunoblots were probed with anti-ICN1 antibody (to visualize Fbw7-bound ICN1). Note that all patient-derived mutants were compromised in their ability to bind Fbw7. Input, whole cell lysates.

f, Mice received wild-type HPC transduced with Notch1-P12 (n=7), Notch1-P12 carrying patient-derived S2514F mutation (n=9) or Notch1-P12 with P2513A, S2514F and P2515R mutations (n=6). Shown is Kaplan-Meier analysis of survival. *P*=0.03 for Notch1-P12 WT vs. Notch1-P12 S2514F; *P*=0.01 for Notch1-P12 WT vs. Notch1-P12 P2513A/S2514F/P2515R (Log-rank test).